Univerzita Karlova v Praze

Přírodovědecká fakulta

Fyzikální chemie

Bc. Marie Kolářová

Dynamická saturační optická mikroskopie používající světlem přepínatelné proteiny

Dynamic saturation optical microscopy using photoswitchable proteins

DIPLOMOVÁ PRÁCE

Školitel: Mgr. Aleš Benda, Ph. D.

Praha, 2011

Prohlašuji, že jsem závěrečnou práci zpracovala samostatně a že jsem uvedla všechny použité informační zdroje a literaturu. Tato práce ani její podstatná část nebyla předložena k získání jiného nebo stejného akademického titulu.

V Praze, 12. 5. 2011

Podpis

Abstrakt

Fluorescenční mikroskopie je nepostradatelnou technikou pro zobrazování živých buněk. Jedním z hlavních omezení této metody je difrakcí světla limitované, relativně malé prostorové rozlišení, což je popsáno Abbeho difrakčním zákonem. V posledních letech se proto začaly rozvíjet techniky, které obchází difrakční limit za účelem zvýšení prostorového rozlišení. Jednou z těchto technik je dynamická saturační optická mikroskopie (DSOM), která je založena na prostorovém sledování kinetiky vratných přechodů mezi svítivými a nesvítivými stavy fluoroforů. Reverzibilní přechod do nesvítivého stavu může být pozorován např. u světlem přepínatelných fluorescenčních proteinů jako je Dronpa a z ní odvozené klony. Zmíněné proteiny opakovaně přecházejí mezi fluorescenčními a nefluorescenčními formami po ozáření modrým nebo ultrafialovým světlem. Tato práce se soustředí na získávání lépe rozlišených fluorescenčních obrazů na základě pozorování kinetiky přechodů v různých částech vzorku. Experimenty byly prováděny na kvasinkách exprimujících proteiny označené Dronpou. Nejdříve bylo ověřeno, zda v Dronpě dochází k přepínání mezi svítivými a nesvítivými stavy. Dále byl sledován vliv intenzity excitační světla a změna excitační vlnové délky na rychlost přepínání a fotostabilita proteinu. Měření byla prováděna na různých časových škálách a s různými proteiny. Závěry z provedených pokusů umožnily optimalizaci experimentálních podmínek pro samotné zobrazování, díky čemuž se podařilo získat obraz vzorku s dvakrát větším prostorovým rozlišením oproti standardnímu konfokálnímu obrazu. Neméně důležité zjištění je, že kromě zvýšení prostorového rozlišení v ohniskové rovině metoda DSOM dokáže vylepšit kvalitu získaného obrazu rovněž odfiltrováním nežádoucí autofluorescence a fluorescenčního signálu pocházejícího mimo ohniskovou rovinu.

Abstract

Fluorescence microscopy is an essential technique for live cell imaging. One of its drawbacks is a rather low diffraction limited spatial resolution, which is described by Abbe diffraction law. Therefore, in the last decade a lot of new methods improving spatial resolution were developed. One of them is dynamic saturation optical microscopy (DSOM) that is based on spatial monitoring of reversible transition kinetics between bright and dark states of fluorophores. The dark state is possible to obtain for example by using reversibly photoswitchable fluorescent proteins such as Dronpa and its variants. These proteins undergo reversible transition from fluorescent to nonfluorescent state after irradiation by blue and ultraviolet light. In my work I focus on employing the kinetics of controllable photoswitching of Dronpa in improving the overall image quality, including the spatial resolution. The experiments were performed on yeasts expressing selected proteins labelled with Dronpa. Firstly, photoswitching behaviour of Dronpa was confirmed. Secondly, experimental conditions were optimized by studying dependence of switching rate on laser intensities and on excitation wavelength and by studying protein photostability. Experiments were performed on different timescales and for various proteins. Using the optimal experimental conditions a DSOM image with two times better spatial resolution in focal plane than classical scanning confocal microscope was obtained. Moreover, background in form of out-of-focal plane fluorescence signal was suppressed as well as autofluorescence, leading to sharper images.

Content

1 Introduction

Microscopy has always served as an important tool for observing tiny details of different structures. One of its branches is fluorescence microscopy which is often used for its favourable properties as high sensitivity, contrast and possibility to selectively highlight parts we are interested in. Furthermore fluorescence microscopy is a non-invasive technique allowing live cell imaging. One of its drawbacks is a rather low diffraction limited spatial resolution, which is described by Abbe diffraction law [1]. Therefore, in the last decade a variety of new methods improving spatial resolution were developed. The most promising methods are stimulated emission depletion microscopy (STED) and variants of photoactivated localization microscopy (PALM). These methods are able to reach resolution under 50 nm with respect to nature of specimen [2-3]. Other introduced methods are structured illumination microscopy (SIM), saturation excitation microscopy (SAX) or super-resolution optical fluctuation imaging (SOFI). All of these methods have specific benefits and limitations; none of them has truly universal utilisation. These methods have already shown that they are able to image cellular structures with sub-diffraction resolution [3-7].

One relatively new method is dynamic saturation optical microscopy (DSOM) [8-9] that is based on spatial monitoring of fluorescence decay caused by fluorophore's transition from fluorescent to non-fluorescent state. DSOM requires using fluorophores in which reversible transition between fluorescent and non-fluorescent states is observable. Transition between first excited singlet state and triplet state of fluorophore or transition between bright and dark state of reversibly photoswitchable fluorescent compounds can be employed. An example of photoswitchable compound is a fluorescent protein Dronpa [10]. Cells' proteins can be specifically labelled with fluorescent proteins using genetic manipulation. Labelling with Dronpa thus enables visualising selected parts of cells and is an appropriate sample for DSOM testing.

The main purpose of this work is to show that dynamic saturation optical microscopy is also an applicable method for sub-diffraction imaging of living cells.

2 The aim of the diploma work

The aim of my work is to obtain high-resolution pictures of biological samples by using DSOM method. High resolution means spatial resolution better than diffraction limit. The first goal comprises the characterization of switching properties of Dronpa, namely:

- Confirmation of light-induced switching behaviour
- Influence of laser power on switching rate
- Determining of fluorophore photostability
- Influence of activation intensity on fluorescence intensity
- Effect of excitation wavelength on switching rate
- Comparison of Dronpa's switching properties with other fluorescent proteins
- Photoswitching on different time scales

The second goal is to acquire highly-resolved pictures. The choice of optimal experimental conditions is based on the results from the first part. This part contains two sections:

- Acquisition of high-resolution images of cells labelled with Dronpa
- Testing of cells labelled with originally non-photoswitchable fluorescent protein for obtaining more resolved pictures

3 Theory

3.1 Resolution of optical microscopy

Resolution of an optical microscope is limited by wave nature of light. The diffraction of light on the sample causes that a small point appears as a blurred spot. An approximate definition of resolution is "the largest distance at which the image of two point-like objects seems to amalgamate" [11]. The way (of distribution of light intensity), how infinitely small point gets imaged by an imaging system, is called point spread function (PSF) (Figure 3.1). In context of PSF, several resolution criteria were suggested. First, often used, measure of resolution is full width of PSF at half maximum (FWHM). Next resolution limit is given by Rayleigh criterion that is defined as a distance between central maximum and first minimum of PSF. Sparrow limit is a distance between two point-like objects with the same intensities just when a dip at half way between them disappears. This resolution limit enables resolution of two points in even closer distance than is given by Rayleigh limit. These limits are defined in real space and are really helpful during visible observation of sample.
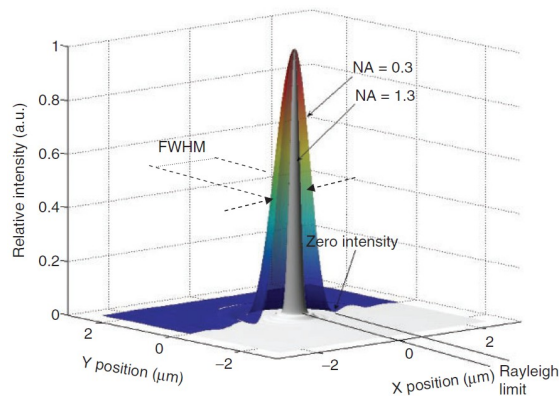
Figure 3.1. Point spread function. Two PSFs are depicted on picture, they differ in numerical aperture NA of objective (term explained later in text). Full width at half maximum and Rayleigh limit are also denoted. Adapted from [12].

A more precise definition was proposed by Abbe [1]: "the Abbe limit corresponds to the distance of the finest periodical structure which can be imaged by an optical microscope" [11]. It is based on the fact that in Fourier space every object can be described as a sum of sinusoidal curves with different spatial frequencies (the number of cycles per meter of a periodic pattern). Higher spatial frequencies contain information

about finer object details, lower frequencies contain information about coarser details. Finer periodic structures are presented in rays that are leaving the specimen in higher diffraction angle, but these rays mostly miss the objective. Numerical aperture NA of objective affects the resolution and can be defined by

$$NA = n \cdot \sin \alpha ,$$ (1)

where n is index of refraction medium between the objective front-lens and the specimen, α is the half-angle of the maximum cone of light that can enter or exit the lens. For widefield fluorescence microscopy the Abbe limit becomes

$$d = \frac{\lambda}{2 NA} ,$$ (2)

where λ is wavelength of light and d is the minimal resolvable distance. According to the Abbe formula, the resolution is about half size of emitted wavelength.

In confocal fluorescence microscopy the diffraction of light causes that the detection volume is not infinitely small. The size of the detection volume is determined by the used excitation wavelength, objective properties and a pinhole. Resolution of a confocal microscope can be enhanced by reduction of the detection volume.

3.2 Brief descriptions of super-resolution microscopy methods

In the last decade, a variety of new techniques that improve both lateral and axial spatial resolution appeared. Focused on lateral resolution, methods can be divided into several groups [8]. First group uses non-uniform illumination of the sample. In structured illumination microscopy [5] (widefield technique), the sample is illuminated with a series of excitation light patterns. The observed image is a product of this pattern and imaged object and contains information about detailed structure of sample which can be extracted by mathematical treatment.

Second group uses saturation of excited state. In stimulated emission depletion microscopy [13] (STED, confocal t.), the sample is illuminated with two laser beams. The first one excites molecules, the second one (STED beam) causes stimulated emission. The second depletion beam has doughnut shape therefore molecules on the border of detection volume are transferred to the ground state. For efficient switching off, high intensity STED beam is needed. Then, only molecules in "the middle of doughnut" can fluoresce and the size of detection volume is substantially reduced. Other method is saturation excitation microscopy [14-15](confocal and widefield t.) in which

very high intensities of irradiation cause saturation of excited state. It means that fluorescence signal is no more linearly proportional to the intensity of excitation. By observing non-linear contributions to fluorescence signal, the resolution can be moderately enhanced.

Third group of techniques employs dark state of the fluorescent compounds. In photoactivated localization microscopy [3, 16] (PALM, widefield t.) or in stochastic optical reconstruction microscopy [17] (STORM, widefield t.), the sample is handled (chemically and/or optically) in such a way that only few fluorophores fluoresce at the same time. Just one fluorescing particle is typically in the diffraction limited area hence the location of this particle can be determined very precisely. After localization procedure, molecules are transferred to non-fluorescent state. Process of irradiation (activation), localization and deactivation repeats many times. The image is then created from thousands of bright points. One of the newest methods is super-resolution optical fluctuation imaging [7] (SOFI, widefield t.). This method relies on higher-order statistical analysis of temporal fluctuations, which are caused by fluorescence blinking, recorded in a sequence of images. The method used in this work is dynamic saturation optical microscopy (DSOM) [8-9]. It relies on the reversible transitions between fluorescent and non-fluorescent states and is based on spatial monitoring of the transition kinetics. The more detailed description of DSOM will follow in next chapter.

3.3 Dynamic saturation optical microscopy (DSOM)

3.3.1 DSOM introduction

DSOM is based on spatial monitoring of transition kinetics between bright and long lived dark states of fluorophores. After a sudden switch on of irradiation, exponential decay of fluorescence can be observed. The fluorescence decay demonstrates dynamic transition from bright state to dark states of fluorophore. The higher excitation intensity is used, the faster transition to dark state occurs. By monitoring the decay rates under inhomogeneous illumination of the sample, higher spatial resolution can be obtained.

DSOM can be in principal combined with both confocal and structured illumination widefield microscopy. This work focuses on confocal realization. DSOM image is obtained by raster scanning of tightly focused laser beam through the sample with confocal detection of the emitted fluorescence light. The focused laser beam

provides the necessary inhomogeneous distribution of excitation light. At every pixel of the image the sample is irradiated with a given laser sequence to obtain the local transition kinetics. The pixel size is chosen according to Nyquist criterion which says that sampling frequency should be at least twice the resolution limit for a given optical system [18]. The obtainable resolution was estimated to 100 nm hence the scanning step (that determines the pixel size) was set to 50 nm.

The standard experimental realization of DSOM method can be roughly summarized as follows: Sample is scanned through focused laser beam with 50 nm step. In every step, the same laser sequence is applied and fluorescence decay due to formation of dark state is measured. Rate of fluorescence decay depends on spatially varying excitation intensity. The faster the decay rate is the closer the fluorophore is located to intensity maximum (centre) of the laser beam. The local contribution of fast decay to the measured local total fluorescence decay can be extracted by multi-exponential fit. Amplitudes corresponding to the fastest decay time (molecules from the centre of the focused laser beam) form the high resolution image.

The more detailed description and mathematical derivation demonstrating DSOM principle will be presented in following chapters. The first chapter describes dynamic processes that can happen after a sudden illumination of a sample. Second chapter mathematically describes kinetics of these dynamic processes. Creation of spatio-temporal image is shown in third chapter and real data analysis is described in chapter four.

3.3.2 Three- and four-state model for fluorophore behaviour

Dynamic processes that can occur after a sudden switch on of excitation light can be described using simplified three-state model (Figure 3.2). Let us consider molecule that can occur in ground state (S_0), first excited state (S_1) and dark state (D). After absorbing of light, molecule is excited from S_0 to S_1 state. Molecule in excited state has two possible ways to follow. First one leads to S_0 state and is accompanied by emission of light. This process occurs during nanoseconds. Second way is transition to dark state followed by activated or spontaneous return to S_0 state. These transitions occur on the longer time scale, e.g. hundreds of microseconds or milliseconds. Because of different time scales, formation kinetics of excited and dark states can be treated independently.
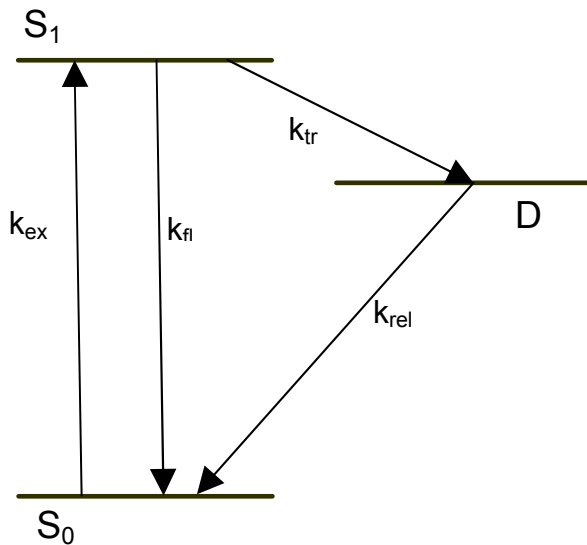
Figure 3.2. Three-state model. S_0 is ground state, S_1 the first excited state, D dark state. k_{ex} is excitation rate constant, k_{fl} fluorescence rate constant, k_{rel} is the dark state relaxation rate constant and k_{tr} the rate constant of transition from S_1 to D state.

The three-state state model can be extended to four-state model in which also existence of triplet state T is considered (Figure 3.3). Such model would be able to describe the kinetics of short-time photoswitching in more detail. The four-state model comprises three processes: fast establishing of equilibrium between S_0 and S_1, slower intersystem crossing to triplet state eventually leading to a steady state and the slowest process – the transition to dark state. The exact mechanism of transition to dark state is usually unknown, therefore transitions both from S_1 and T should be considered. The four-state model can be described by kinetic equations in analogical way as the three-state model (the kinetic equations of the three-state model are solved further in the text). Considering the dynamics of the dark state, it behaves in the same way as the three-state model, since all other processes are much faster and the steady state is established quickly. Therefore, it can be effectively replaced by the three-state model with new rate constants. Relations between the rate constants of four-state and modified three-state model can be derived.
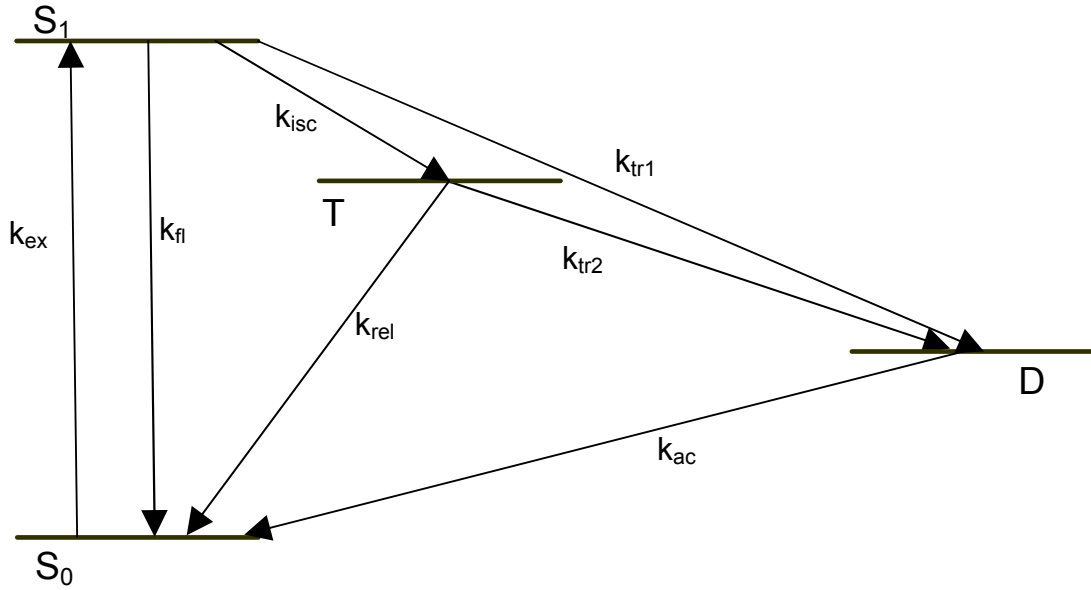
Figure 3.3. Four-state model. S_0 is ground state, S_1 is first excited state, T triplet state, D dark state. k_{ex} is excitation rate constant, k_{fl} fluorescence rate constant, k_{isc} the intersystem crossing rate constant, k_{rel} the triplet state relaxation rate constant, k_{tr1} the rate constant of transition from S_1 to D state, k_{tr2} the rate constant of transition from T to D state and k_{ac} is the dark state relaxation rate constant.

3.3.3 Kinetics of singlet and dark states formation

Derivation of kinetics of different state formation, creation of spatio-temporal image and data analysis will cite and follow an article of Jana Humpolíčková [8]. Mathematical derivation is done for three-state model.

After a sudden switch-on of illumination light with constant intensity at time $t = 0$, fast pre-equilibrium between the S_0 and S_1 state is established. "The dependence of the steady-state probability of finding a molecule in the excited state S_1 (provided that no dark state is formed) on the excitation rate k_{ex} is:

$$S_1\left(t \gg \frac{1}{k_{fl} + k_{ex}}\right) = \frac{k_{ex}}{k_{fl} + k_{ex}} = K \,, \tag{3}$$

where k_{fl} is the rate constant of the excited singlet-to-ground state transition (fluorescence). As it was already mentioned, this steady state is reached after few nanoseconds and provides the initial condition for the subsequent dark state formation which occurs on millisecond timescale τ. The evolution of the probability that a molecule is in the dark state D is described by the equation:

13

$$\frac{dD(\tau)}{d\tau} = k_{tr}S_1(\tau) - k_{rel}D(\tau),\tag{4}$$

where k_{tr} is the rate constant of transition from S$_1$ to D and k_{rel} is the dark state relaxation rate constant. The probability of having a molecule in the S$_1$ state on the millisecond timescale is a product of the steady-state probability of $S_1(t)$ given by Eqn. (3) and the probability function $\alpha(\tau)$, which describes the depopulation of both the singlet ground and excited states. The probability of finding a molecule in the S$_1$ state is therefore: $S_1(\tau) = \alpha(\tau)K$. Taking into account the fact that one has $\alpha(\tau) + D(\tau) = 1$, the temporal fading of the S$_1$ state at time τ after the laser has been turned on is the following:

$$S_1(\tau) = K\frac{k_{rel} + k_{tr}Ke^{-(k_{rel}+k_{tr}K)\tau}}{k_{rel} + k_{tr}K}\text{ ” [8]}.\tag{5}$$

This relation describes a decay of S$_1$ state due to formation of dark state. This decay approves itself as fluorescence decay. The higher intensity of excitation (involved in K) is applied the more rapid formation of dark state occurs.

Eqn. 5 describes time evolution of probability S_1. Assignment of this probability to fluorophores distributed in space enables creation of spatial image containing temporal information.

3.3.4 The spatio-temporal image

"Mathematically expressed, the spatio-temporal image $im(\vec{r}, \tau)$ becomes a convolution of the fluorophore's concentration pattern $c(\vec{r})$ and the spatial profile of the temporally evolving probabilities $S_1(\vec{r}, \tau)$:

$$im(\vec{r}, \tau) = k_{fl}\int c(\vec{r}')S_1(\vec{r} - \vec{r}', \tau)d\vec{r}'\,.\tag{6}$$

After insertion of Eqn. (5) into Eqn. (6), the spatio-temporal image of the observed fluorescence pattern becomes:

$$im(\vec{r}, \tau) = I_{stac}(\vec{r}) + k_{fl}\int c(\vec{r} - \vec{r}')K(\vec{r}')\left(1 - \frac{k_{rel}}{k_D(\vec{r}')}\right)e^{-k_D(\vec{r}')\tau}d\vec{r}'\tag{7}$$

The temporally independent part of the expression, I_{stac} equals

$$I_{stac}(\vec{r}) = k_{fl}\int c(\vec{r} - \vec{r}')K(\vec{r}')\frac{k_{rel}}{k_D(\vec{r}')}d\vec{r}'\,,\tag{8}$$

where k_D is the intensity dependent rate constant of transition to D state:

$$k_D(\vec{r}) = k_{rel} + k_{tr}K(\vec{r})\text{''} \quad [8]. \tag{9}$$

For now, the concept of a group of fluorophores will be left and on just one fluorophore irradiated by focused laser beam will be examined. At first, we can consider that fluorescing molecule is scanned in one dimension only. The laser intensity profile is Gaussian, as was already mentioned. The obtained fluorescent profile is also Gaussian. When the scanning is repeated after a period of time, the lowering of profile intensity can be observed (Figure 3.4, left). The largest changes occur in the middle of fluorescence profile, the less evident changes are on the borders of profile. The Figure 3.4, left shows evolution of intensity profile in time. This temporal evolution can be converted into spatial dependence where fluorescence decays are measured at different positions. (Figure 3.4 right). The most rapid fluorescence decay is obviously observed when molecule is in the intensity maximum of laser beam. It means that the rate of fluorescent decay bears information about position of fluorescing molecule. This information can be used for resolution enhancing.
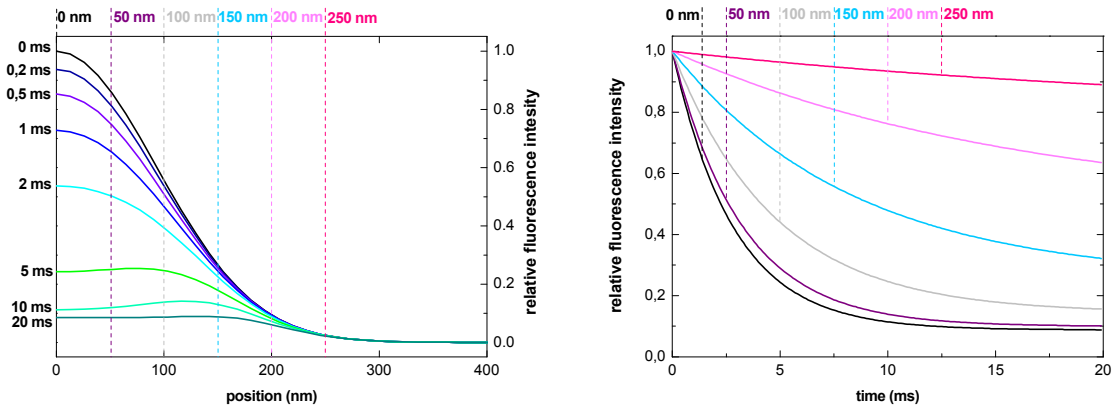
Figure 3.4. Left: Evolution of fluorescence intensity profile in time. Right: Fluorescence decays in different position to laser centre.

In theory, scanning of fluorescent molecule in two dimensions creates an image composed of infinitely thin concentric circles. Every circle represents areas where the same decay rates k_D can be observed. It means that the image can be obtained by integration of spatial contributions with a given value of k_D. That was firstly expressed in Eqn. 7, calculation of the finite integral can be performed as an infinite sum of contributions with a given value of k_D and this can be approximated by summation

$$im(\vec{r},\tau) = \int_0^{k_{D_{max}}} A(k_D \mid \vec{r})e^{-k_D(\vec{r})\tau}dk_D \approx \sum_{i=1}^{n} A\left(k_D \in \left\langle k_{D_i}, k_{D_i} + \Delta k_D \right\rangle \mid \vec{r}\right)e^{-k_{D_i}\tau}\Delta k_D + A(\vec{r}), \quad (10)$$

where $A(k_D \mid \vec{r})$ is spatial contribution with transition kinetics k_D, $A(\vec{r})$ is the temporally constant offset. Right side of Eqn. 10 describes the image as a finite sum of contributions with range of k_D. It means that the acquired image is composed of concentric circles with definite thickness. The smallest radius belongs to the fastest decay rates, which can be observed in the vicinity of intensity maximum. Monitoring of fast decay rates enable molecule's localisation. The precision of localisation depends on the number of detected photons and on the resolution of k_D values, which is given by the temporal resolution of the dynamic experiment. The radius of the smallest (central) circle defines the obtainable resolution.

3.3.5 Data analysis

Fluorescence decay is obtained in every scanned pixel. Data from every pixel can be fitted to model of several exponentials (Eqn. 10). For real data analysis, two exponentials are enough. Data are fitted by non-negative least square method to two exponential model with given decay times τ_{fast} and τ_{slow}:

$$im(\vec{r},\tau) = A_{fast}(\vec{r})\exp\left(-\frac{\tau}{\tau_{fast}}\right) + A_{slow}(\vec{r})\exp\left(-\frac{\tau}{\tau_{slow}}\right) + A(\vec{r}) \quad\quad (11)$$

where $A_{fast}(\vec{r})$ forms the high-resolution image corresponding to the fast transition kinetics. Fast transition kinetics is described by the short decay time τ_{fast}, which was established before fitting procedure and is unvaried for all positions $\vec{r}$. $A_{slow}(\vec{r})$ is the kinetic image assigned to the long decay time τ_{slow}, which was also chosen before fitting procedure. $A(\vec{r})$ is the kinetic image assigned to temporally constant offset. Temporally constant offset comes from contributions with constant fluorescence signal. Image corresponding to slow decay component behaves as mathematical iris-like aperture that screen out all the kinetic contributions that are not fast enough. The choice of τ_{fast} and τ_{slow} determines the fraction of photons that are used to create high resolution image and this choice also influences the obtainable resolution.

3.4 Dark states of fluorophores

As was already mentioned, some super-resolution methods make use of fluorophores blinking. Blinking is caused by reversible transition between bright and dark states. These transitions are usually induced by light. Dark states can be obtained in several ways. One way is to use intrinsic states of fluorophores as triplet state formation. The other way is to use photoswitchable compounds. Ideal photoswitches have two thermally stable and spectrally separated states. Further, ideal photoswitches show high fluorescence quantum yield, low photobleaching tendency and high switching efficiency. Unfortunately such photoswitches do not exist. Currently existing photoswitches can be divided into three groups [19]: reversibly photoswitchable fluorescent proteins, organic dyes and synthetic conjugates.

Reversibly photoswitchable proteins are naturally occurring proteins derived from mutants of GFP-like fluorescent proteins. Cell labelling with fluorescent proteins enable highlighting sub-cellular structures or even visualizing proteins' movements. The drawback is low photostability and size which can influence the function of bounded protein. The most discussed and used reversibly photoswitchable fluorescent protein is Dronpa [10]. This protein can be repeatedly converted between fluorescent and nonfluorescent state by irradiation with blue and ultraviolet light.

Besides photoswitchable proteins, photoactivable and photoconvertible fluorescent proteins exist. These proteins also undergo transition between two different states but the transition is irreversible (it can happen only once). Photoactivable proteins, e.g. PA-GFP [20], need activation, typically by light, to manifest the fluorescence. Photoconvertible proteins can be found in two different fluorescent states, the transition between them is induced by light activation. An example is mEOS [21] that emits green light in native state and red light in photoconverted state.

Organic dyes as carbocyanine fluorophores (Cy5, Cy7 or Alexa647) [22-23] have shown photoswitching behaviour under specific conditions as removal of oxygen, presence of thiol compounds or presence/absence of activator. Their advantage over fluorescent proteins is high photostability enabling to emit higher number of photons. Protein labelling is also available.

Organic synthetists were partly successful in developing photoswitchable compounds. The most promising compounds are diarylethene derivatives with heterocyclic aryl groups [24] and spiropyrans [25]. These photoswitches show extreme

photostability but very weak fluorescence. Interesting usage of synthetic compounds is as Föerster resonance energy transfer acceptors that can reversibly switch the fluorescence of a donor fluorophore.

Cell's imaging requires labelling with fluorescent molecules. The easy way how to specifically label cell structures is usage of fluorescent proteins. In this work, Dronpa and its mutant are used.

3.4.1 Dronpa

Dronpa is a mutant of GFP-like fluorescent protein derived from coral Pectinidae. This reversibly photoswitchable fluorescent protein can be repeatedly converted between fluorescent and nonfluorescent state by irradiation with two different wavelengths. Excitation with blue light causes fluorescence in green region of spectrum (Figure 3.5) and also switching to dark (nonfluorescent, off-state) state. Return to bright (fluorescent, on-state) state is induced by irradiation with ultraviolet light. Spontaneous relaxation from dark to bright state is also observed but is very slow. Basic switching characteristics are written down in Table 3.1.
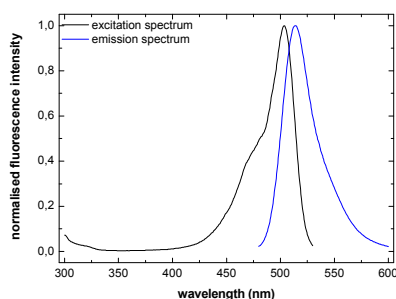

Figure 3.5. Excitation and emission spectra of Dronpa. Spectra are adapted from [26]

Table 3.1

Fluorescent protein	Absorption max. on/off state (nm)	Emission max. (nm)	Extinction coeff. ($M^{-1} cm^{-1}$)	Fluorescence quantum yield
Dronpa	503/392	518	95000	0,85
rsFastLime	496/384	518	39094	0,77

Fluorescent protein	Fluorescence lifetime (ns)	Off-state fluorescence	Bleaching per cycle	Relaxation half-time (min)	Equilibrium (% fluor. max.)
Dronpa	3,6	6%	17%	840	100
rsFastLime	2,7	1,5%	2%	8	93

Data are adapted from [10, 27-28].

"Dronpa exhibits a typical GFP-like fold, comprising an eleven-stranded β-barrel with a co-axial partially helical element that bears the chromophore" [29] (Figure 3.6). The chromophore is formed spontaneously from the tripeptid CYG (Cys-62, Tyr-63, Gly-64) (Figure 3.6). It was shown that the chromophore adopts deprotonated cis configuration in its bright state and protonated trans configuration in its dark state. Furthermore, Dronpa exists in an acid-base equilibrium, but only the photoinduced protonated form shows switching behaviour.
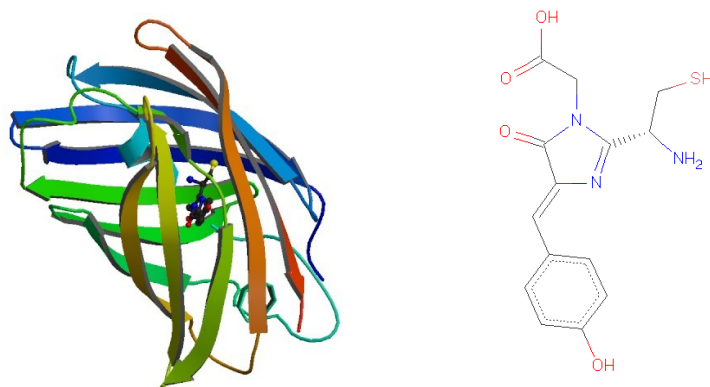

Figure 3.6. Left: Crystal structure of Dronpa. Right: Chromophor formed from CYG. Adapted from [30].

The exact mechanism of transition from off to on-state and back is still unknown. Based on cis-trans isomerization and change of protonation state, two possible mechanisms were suggested. The first model proposes a cis-trans isomerization of the chromophore as primary event of the switching process that is accompanied by several residue rearrangements [31]. Upon cis-trans isomerization, the chromophore is exposed to different local environments with distinct electrostatic surface potentials. These differences influence chromophoric protonation and determine that the fluorescent form is deprotonated (anionic) and nonfluorescent state is protonated (neutral). Cis-form of chromophore is predominantly deprotonated and therefore fluorescent, trans-form is predominantly protonated and therefore nonfluorescent. The second model stresses the importance of proton transfer and suggests the route of proton movement [32]. Protonation state of chromophore is closely connected to flexibility of surrounding structure. Flexibility of chromophore determines fluorescence or nonfluorescence of Dronpa. In this model cis-trans isomerization is not necessary. Models are based on crystallographic and NMR studies [29, 31-32], which revealed stabilization of chromophore by hydrogen bond between the chromophore hydroxyl oxygen and hydroxyl group (Ser-142) on the barrel wall (Figure 3.7). This hydrogen

bond helps to hold the rings of chromophore in a cis-configuration. The interaction between imidazole ring of His-193 and phenyl moiety from chromophore holds the whole chromophore in a coplanar conformation. This rigid structure favours the radiative transition from the first excited electronic state to the ground state. By contrast, in the dark state, that hydrogen bond and stabilization by imidazole ring are missing. The flexibility of chromophore and neighbouring part of β-barrel increases and leads in favouring of nonradiative relaxation processes.
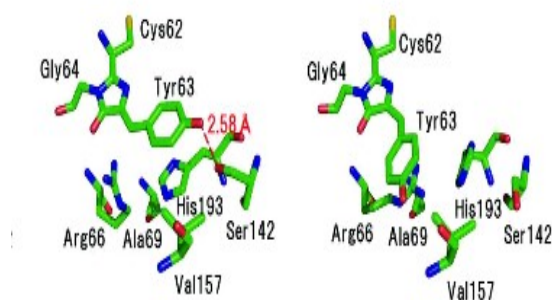

Figure 3.7. Stick models of the chromophore and nearby residues. Left: on-state, right: off-state. Adapted from [33].

Photoswitching of Dronpa can be observed by monitoring fluorescence decay. Rate of photoswitching can be controlled by intensity of irradiation light (blue or UV light). On-times, which correspond to time that molecule spends in bright state before converting to dark state, are intensity dependent and are usually observed on millisecond or second time scale. It was also shown that photoswitching can occur within tens of microseconds [34]. Measurements of fluorescence intensity trajectories (done by Habuchi et al. [35]) showed that molecules of Dronpa can dwell some time at some form of dark state. During this time (off-time) molecule can not fluoresce. In that work three types of off-times were observed: long off-time (in order of tens of seconds), medium off-time (in order of tens of milliseconds) and short off-time (around one millisecond). The long off-time was attributed to spontaneous transition from dark to bright state (this time was shortened due to duration of experiment). The medium off-time was attributed to another dark state that was not further specified. The short off-time was related to transition into triplet state.

Photoswitching behaviour is summarised in one of proposed schematics (Figure 3.8).
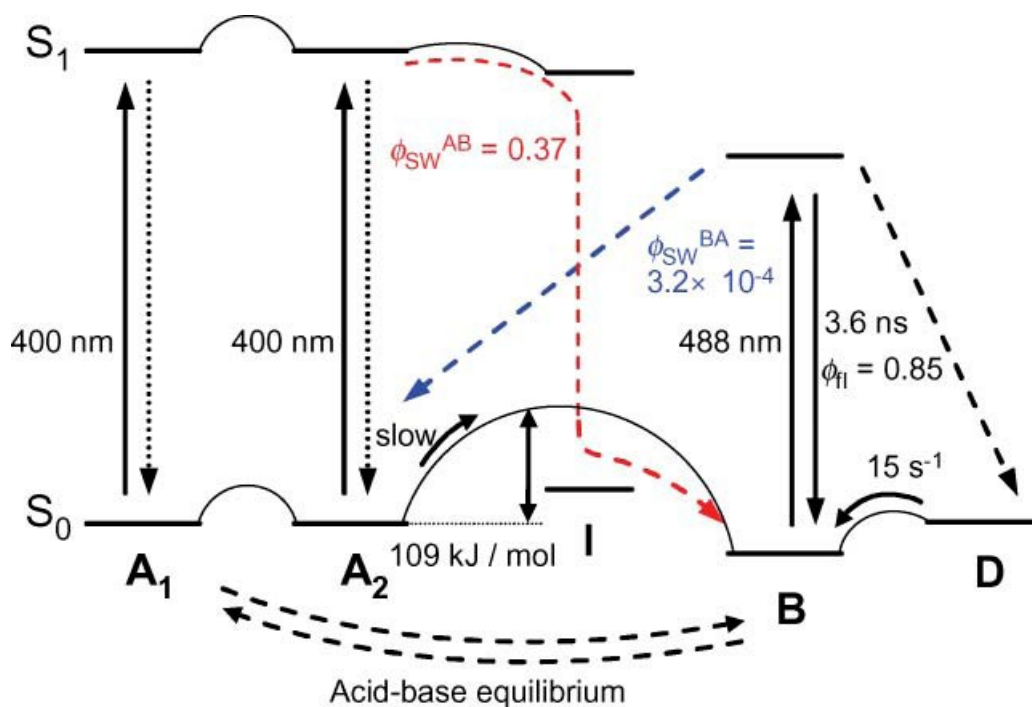
Figure 3.8. Proposed schema of photoswitching. B is deprotonated state, A_1 is protonated state and A_2 is photoswitched protonated state, D is another dark state, I is intermediate state, ϕ_{fl} is fluorescent quantum yield, ϕ_{SW}^{AB} is quantum yield of photoswitching from A_2 to B, ϕ_{SW}^{BA} is quantum yield of photoswitching from B to A_2. A_1 and B are in acid-base equilibrium. Irradiation of bright B state with light of 488 nm causes fluorescence and transition to dark state A_2. States A_2 and A_1 are not interconvertible probably because of distinct protein environment. Activation of A_2 state by UV light causes transition from dark state to bright state. This transition is suggested to occur via intermediate state I. Spontaneous recovery from A_2 to B state is slow because of relatively large activation energy. Existence of another dark state D is probable. Figure is taken from [35].

Extraordinary switching properties of Dronpa led to introducing mutations into genetical code and creating new variants of Dronpa, e.g. rsFastLime [29] (Dronpa-V157G, spectral characteristics in Table 3.1). rsFastLime also shows photoswitching behaviour. In comparison with Dronpa, switching to dark state is more efficient, it means that the switching kinetics is faster. Bleaching per cycle is reduced, spontaneous relaxation to ground state is faster.

4 Materials and methods

4.1 Confocal microscopy

The experiments were performed with a home-built confocal optical setup based on the inverted microscope IX71 (Olympus, Hamburg, Germany). The excitation light, 458, 466, 473, 477, 488, 496 nm lines of Ar-ion laser, passes through an acousto-optical tunable filter (AOTF) and an acousto-optical modulator (AOM) (AOTFnC-400.650 and MT200-A0,5-VIS, AAOptoelectronic, Orsay, France). The UV excitation light, continuous mode of diode laser (LDH-D-C-400B, 405 nm, PicoQuant), passes through an acousto-optical modulator (MQ110-A0,7-UV, AAOptoelectronic, Orsay, France). The AOTF selects the wavelength and intensity and the AOM can vary the intensity and creates sharp (tens of ns rise time) rectangular pulses. The intensity modulated laser beams are overlapped using dichroic mirror (LM01-427-25, Semrock, Rochester, NY) and coupled into a single-mode polarization-maintaining optical fiber (Schafter-Kirchhof, Germany) for spatial mode filtering. Re-collimation is done with an air-spaced objective (UPLSAPO 4X, Olympus), and the collimated laser beam enters the back port of the microscope body. The microscope itself contains the standard confocal part consisting of a main dichroic mirror (ZT405/488/638rpc, Chroma, Rockingham, VT or FF509-FDi01, Semrock, Rochester, NY), a water immersion objective (UPLSAPO 60x, Olympus), 3D sample scanning stage (PIMars XYZ NanoPositioner, 200x200x200 μm, PI, Karlsruhe, Germany), 50 μm diameter pinhole placed at the focal plane of the left camera port, a recollimation lens, and an LP500 emission filter (Chroma). All optomechanical components were bought from Thorlabs (Newton, NJ). In contrast to standard confocal setups, the detection unit is an EM-CCD camera (DU-860D-CS0-#BV iXon 128x128 pixels, Andor, Belfast, United Kingdom). The reason for choosing EM-CCD camera as a point detector is its high sensitivity, superior linearity and high dynamic range. It allows detection in ranges from single photons to millions of photons per time unit without need for any "saturation" correction. The projected image of the pinhole on the EMCCD is made smaller by a factor of 5 to fit into a single pixel (24 μm x 24 μm) close to the bottom of the light sensitive part of the chip.

Two implemented ways of data readout were used in this work. In the first mode, called intensity scan, the camera is synchronized with scanner clock (5 kHz) and

reads out data from a 3x3 binned single line (20 pixels), containing the illuminated pixel, every 200 μs (5 kHz). The excessive blank pixels are used for background correction. In combination with synchronized modulation of excitation intensity this mode enables performing time-laps experiments at every pixel of the final image with 200 μs time resolution and almost arbitrary excitation profile. The dead time for this read-out mode is only 20 μs (image shift on the camera), for which we correct by intermitting the excitation light during the dead time period.

To capture faster dynamics, so called image shifting mode was used. The excitation light is switched off until the camera starts to read out an image using a frame transfer mode. As the blank image starts moving down the chip, excitation is switched on and the time evolution of the signal is inscribed along a vertical direction on the EMCCD chip. The time resolution is given by the available camera vertical line clock (from 88 to 450 ns), the maximum number of time points is given by number of pixels on the camera chip (128). We usually used 450 ns vertical clock and 128 pixels for measuring decays lasting about 50 μs. Afterwards, the shifted image is binned 3x1 and read out in a standard way using the EM register. For each horizontal line (time point), the fluorescence signal that is contained in a single binned pixel is corrected for variable camera background using non-illuminated pixels in that line. It takes in total 3 ms to record and store one 128 pixel decay, which sets the speed limit for scanning.

Software for hardware operation and data collection is a home-written program under LabVIEW 2010 (National Instruments) development interface. Routines for data analysis are home-written macros in Matlab R2009b (Mathworks).

4.1.1 Experimental settings

Figure 5.2 with explanations

Yeasts: Dronpa: membrane, rsFastLime (two kinds of cells), 4 days of cultivation on GM medium.

Lasers: 405 nm: Power: 2 μW for Dronpa, 1 μW for rsFastLime. Powers were measured at sample location. (Switched on) ON: curve 1: 0 - 0,4 ms, 4 - 4,4 ms, curve 2: 0 - 0,4 ms, curve 3: switched off.

488 nm: Power: 10 μW for Dronpa, 5 μW for rsFastLime. ON: 0,4 - 4 ms, 4,4 - 8 ms for all curves.

40 points per pixel (ppp) - length of laser sequence applied to every pixel. One point lasts 200 μs (time resolution of scanner and CCD camera). At every pixel, sample is irradiated with laser sequence lasting 8 ms in this case.

100x100 pixels, 100 nm step size - new laser sequence starts every 100 nm of scanner movement. Pixel of the image sample is 100 nm x 100 nm large, the sample is scanned in area of 100 μm^2.

Figure 5.3

Yeasts: Dronpa: cytoplasm, rsFastLime, 5 days.

Lasers: 405 nm: Power: 0,7 μW. ON: 0 - 0,4 ms, 6 - 6,4 ms.

488 nm: Power: (1) 1 μW, (2) 5 μW, (3) 10 μW, (4) 20 μW, (5) 50 μW, (6) 100 μW, (7) 200 μW, (8) 400 μW. ON: 0,4 - 6 ms, 6,4 - 12 ms.

60 ppp, 50x50 pixels, 200 nm step size.

Figure 5.4

Yeasts: Dronpa: cytoplasm, rsFastLime, 3,5 days.

Lasers: 405 nm: Power: 2 μW. ON: 0 - 0,4 ms, 2 - 2,4 ms.

488 nm: Power: 10 μW, pulse lenght: (1) 100 ns, (2) 200 n s, (3) 300 ns, (4) 400 ns, (5) 600 ns, (6) 800 ns, (7) 1200 ns, (8) 1900 ns. ON: 0,4 - 2 ms, 2,4 - 4 ms.

20 ppp, 50x50 pixels, 200 nm step size.

Figure 5.5

The same as Figure 5.3, five scans.

Figure 5.6

Yeasts: Dronpa: cytoplasm, rsFastLime, 3-4 days.

Lasers: 405 nm: Dronpa: ON: 0 - 0,6 ms, 6 - 6,6 ms. Power: 0 - 0,6 ms: 0 nW, 100 nW, 200 nW, 300 nW, 400 nW, 500 nW, 1 μW, 2 μW, 4 μW, 5 μW, 6 - 6,6 ms: 500nW.

405 nm: rsFastLime: Power: 0 - 0,4 ms: 0 nW, 100 nW, 200 nW, 300 nW, 400 nW, 500 nW, 700 nW, 1 μW, 2 μW, 5 μW, 6 - 6,4 ms: 1 μW. ON: 0 - 0,4 ms, 6 - 6,4 ms.

488 nm: Power: 10 μW. ON: 0,6 - 6 ms, 6,6 - 12 ms.

60 ppp, 50x50 pixels, 200 nm step size.

Figure 5.7

Yeasts: Dronpa: membrane, rsFastLime, 4-5 days.

Lasers: 405 nm: Power: 1 µW for Dronpa, 0,5 µW for rsFastLime. ON: 0 - 0,2 ms, 2,2 - 2,6 ms, 4,6 - 5,4 ms, 7,4 - 10 ms.

488 nm: Power: 10 µW for Dronpa, 5 µW for rsFastLime. ON: 0,2 - 2,2 ms, 2,6 - 4,6 ms, 5,4 - 7,4 ms, 10 - 12 ms.

60 ppp, 100x100 pixels, 50 nm step size.

Figure 5.8

Yeasts: Dronpa: cytoplasm, rsFastLime, 4 days.

Lasers: 405 nm: Power: 1 µW. ON: 0 - 0,4 ms, 6 - 6,4 ms.

458 nm, (2) 466 nm, (3) 473 nm, (4) 477 nm, (5) 488 nm, (6) 497 nm: ON: 0,4 - 6 ms. Power: 10 µW.

488 nm: ON: 6,4 - 12ms. Power: 10 µW.

60 ppp, 50x50 pixels, 200 nm step size.

Figure 5.9

Yeasts: Dronpa: cytoplasm, 4 days.

Left: Lasers: 405nm: Weak power: < 60 nW, ON: 0 - 0,4 ms, 6 - 6,4 ms.

466 nm: Power: 30 µW. ON: 0,4 - 6 ms.

488 nm: ON: 6,4 - 12 ms.

Right: Lasers: 458 nm, 466 nm, 473 nm, 477 nm: ON: 0,2 - 2 ms, 4,2 - 5 ms, 7,2 - 7,6 ms. Power: (1) 458 nm: 15 µW, (2) 466 nm: 20 µW , (3) 473 nm: 20 µW, (4) 477 nm: 10 µW.

488 nm: ON: 2,2 - 4ms, 5,2 - 7 ms, 7,8 - 9,6 ms, 10,2 - 12 ms. Power: 10 µW.

60 ppp, 50x50 pixels, 200 nm step size.

Figure 5.10

Yeasts: Dronpa: cytoplasm, 4 days.

Lasers: 405 nm: Weak power: < 60 nW, ON: 0 - 0,4 ms, 6 - 6,4 ms.

488 nm: ON: 6,4 - 12 ms. Power: 3 µW.

497 nm: ON: 0,4 - 6 ms. Power: 3 µW.

60 ppp, 50x50 pixels, 200 nm step size.

Figure 5.11

Yeasts: GFP, unlabelled cells, 3 days.

Lasers: 405 nm: Power: 1 μW. ON: 0 - 0,4 ms, 6 - 6,4 ms.

488 nm: Power: (1) 1 μW, (2) 5 μW, (3) 10 μW, (4) 20 μW, (5) 100 μW. ON: 0,4 - 6 ms, 6,4 - 12 ms.

60 ppp, 50x50 pixels, 200 nm step size.

Figure 5.12

Yeasts: GFP, unlabelled cells, Dronpa: membrane , rsFastLime, 3,5 days.

Lasers: 405 nm: Power: 1 μW (left) and 0,15 μW (right). ON: 0 - 0,4 ms, 4 - 4,4 ms.

488 nm: Power: 5 μW (left) and 2 μW (right). ON: 0,4 - 4 ms, 4,4 - 8 ms.

40 ppp, 100x100 pixels, 50 nm step size.

Figure 5.13

Yeasts: Dronpa: cytoplasm, rsFastLime, 4 days.

Lasers: 405 nm: Power: 5 μW for Dronpa, 2,5 μW for rsFastLime.

488 nm: Power: (1) 13 μW, (2) 33 μW, (3) 46 μW, (4) 66 μW.

50x50 pixels, 100 nm step size.

Figure 5.14

Yeasts: Dronpa: cytoplasm, rsFastLime, 4 days.

Lasers: 405 nm: Power: 5 μW for Dronpa, 1 μW for rsFastLime, no UV before third decay.

488 nm: Power: 66 μW.

50x50 pixels, 100 nm step size.

Figure 5.15-5.17

Yeasts: Dronpa: membrane, 3,5 days.

Lasers: 405 nm: Power: 1 μW. ON: 0 - 0,4 ms.

488 nm: Power: 2 μW. ON: 0,4 - 4 ms.

40 ppp, 100x100 pixels, 50 nm step size.

Figure 5.18

Yeasts: GFP, 3,5 days.

Lasers: 405 nm: Power: 1 µW. ON: 0 - 0,4 ms, 4 - 4,4 ms.

488 nm: Power: 10 µW. ON: 0,4 - 4 ms, 4,4 - 8 ms.

40 ppp, 100x100 pixels, 50 nm step size.

4.2 Used microorganisms

Yeast strains

Saccharomyces cerevisiae BY4742

　　MATα, his3, ura3, leu2, lys2

- used to control autofluorescence background

Saccharomyces cerevisiae BY4742

　　MATα, his3, ura3, leu2, lys2, JEN1-GFP::SpHIS5

- membrane signal of GFP

Saccharomyces cerevisiae BY4742

　　MATα, his3, ura3, leu2, lys2, MAP2-Dronpa::URA3

- membrane signal of Dronpa

Saccharomyces cerevisiae BY4742

　　MATα, his3, ura3, leu2, lys2, MET17-Dronpa::URA3

- cytoplasmic signal of Dronpa

Saccharomyces cerevisiae strain bearing plasmid with rsFastLime fluorescence protein joined with targeting sequence to mitochondria

- mitochondrial signal of rsFastLime

Solid media

(distilled water was used for media preparation)

YEPG (Yeast Extract Peptone Glucose)

1% yeast extract (Imuna)

1% peptone (Imuna)

2% agar (fa KULICH HK)

2% glucose (sterilised separately)

GM (Glycerol Medium)

1% yeast extract (Imuna) (pH set to 5 before sterilisation, sterilised separately)

2% agar (fa KULICH HK)

3% glycerol

30 mM $CaCl_2$ (sterilised separately)

Liquid medium

(distilled water was used for medium preparation)

Storage medium for yeast cells

1% yeast extract (Imuna)

3% glycerol

Agarose gel

0,7% agarose

distilled water

Yeast strains and media were prepared by Dita Strachotová and Aleš Holoubek from Faculty of Science, Charles University in Prague.

Sterilisation

Mediums and toothpicks were sterilised in autoclave for 20 min in 120 kPa.

Storage

Yeast strains were kept in storage medium for yeast cells in -20°C freezer.

Cultivation

Cells were cultivated on solid mediums in thermostat in 28°C (1-2 days on YEPG medium, then 3-6 days on GM medium).

Preparation of cells for imaging

The live yeast cells were suspended in water and a drop of the suspension was placed on the coverslip and covered by a layer of freshly prepared agarose gel.

5 Results and discussion

Results can be divided into two sections. First section considers characterisation of Dronpa properties and also properties of Dronpa mutant: rsFastLime. At first, suitability of Dronpa for DSOM experiments has to be verified. The verification consists of observation of photoswitching behaviour and dependence of switching rate on laser power. Then, other properties as influence of excitation wavelength, influence of activation intensity, photostability and timescale for observing photoswitching, are tested. Comparison with another non-switchable fluorescent protein is also made. Results from these experiments enable us to optimize experimental conditions for obtaining more resolved pictures. Second part contains acquiring of high resolution images.

All measurements were done on living cells therefore the measurements were affected by cells' conditions as age or measure of expression of fluorescent proteins. The absolute values (absolute fluorescence signal) obtained from experiments were difficult to compare so most of the depicted decays were normalised to one. Most of the measurements were performed with internal calibration so that they were comparable among each other. It means that laser sequence had two parts: one part was the same for all measurements (reference part), second part contained change of one parameter. Measurements were subsequently scaled according to the reference part.

For the sake of simplicity, irradiation with UV light will be called activation and irradiation with blue light will be called excitation. All fluorescence decays presented in this work are averages of all decays from all pixels. The details of shown figures can be found in the Chapter 4.1.1, only information relevant to the text is kept in figure's legend in this chapter.

5.1 Characterisation of Dronpa properties

5.1.1 Confirmation of light-induced switching behaviour

At first, photoswitching was confirmed. During experiment every pixel was irradiated with following laser sequence (Figure 5.1): 400 μs of activation light, 3,6 ms of excitation light and again 400 μs of activation light, 3,6 ms of excitation light.
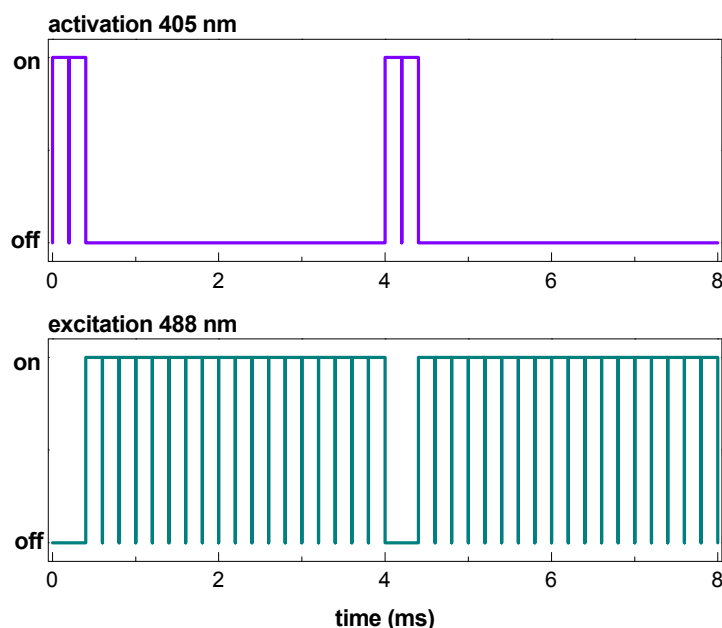
Figure 5.1. Applied laser sequence. Alternation of activation and excitation periods.

Averaged response of the sample can be seen in Figure 5.2. During first activation part only weak fluorescence is observed. This signal comes mainly from autofluorescence of cells. Then, decay of fluorescence is monitored which signalises Dronpa switching from on to off-state. During second activation, the same level of fluorescence can be observed as during first activation period. Activation enables Dronpa return from off to on-state as can be seen in full recovery of fluorescence intensity in second decay (Figure 5.2, curve 1). Fluorescence intensity in the second decay is of the same level as in the first decay. When second activation period is missed then there is almost no recovery of fluorescence signal (Figure 5.2, curve 2). It means that no rapid spontaneous activation happens and first decay seems to continue in second decay. In case that both activation periods are missing, no measurable decay of fluorescence, except a small dip at first two point, is observed because all molecules are switched to dark state maximally once and no recovery occurs (Figure 5.2, curve 3). The small dip at the beginning can be attributed to switching to another short-lived dark state, probably a triplet state. In summary, efficient reversible switching can be only observed when using both activation and excitation light.
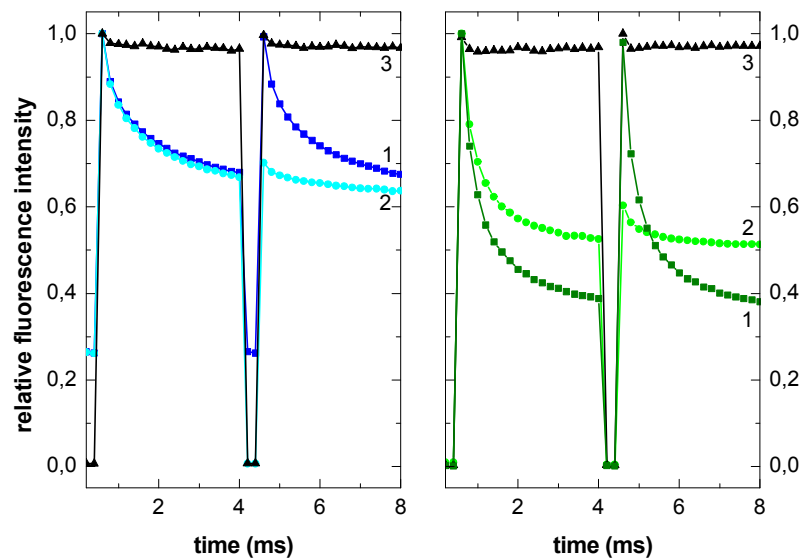
31

Figure 5.2. Photoswitching behaviour of Dronpa (left) and rsFastLime (right). (1) both activations periods were applied, (2) one activation period and (3) no activation period was used.

The same experiment was repeated for rsFastLime. The response of the sample (Figure 5.2) was the same as in the case of Dronpa. When both activation periods were involved, rsFastLime was effectively switched between off and on-states and back as can be seen in two fluorescent decays of nearly identical shape. When one activation period was missing, no efficient switching was monitored. Small increase of fluorescence signal in the beginning of second decay can be caused by diffusion of rsFastLime in mitochondria, by spontaneous thermal activation or return from another short lived dark state (triplet). This increase was not usually present during Dronpa measurements. One reason is that original Dronpa in dark state is very stable and has a very low thermal recovery. Secondly, Dronpa is attached to membrane protein at this particular case whose mobility is restricted hence measurements were not so much affected by diffusion. When no activation periods are used for rsFastLime irradiation then no decay of fluorescence is observed except small dip at first two points caused by the short-lived dark state, similarly to Dronpa. This can be summed up in this way: reliable and efficient switching of rsFastLime is observed only in the case that both excitation and activation light is used.

These measurements confirmed that Dronpa and rsFastLime undergo transitions between dark and bright states so they both behave as an appropriate fluorophore for DSOM experiments.

A question why reversible switching behaviour is needed might be asked. DSOM relies on dynamic processes between bright and dark states. The transition between these states is induced by light. In high-resolution experiment, the size of scanning step must be smaller than size of focused laser beam, diameter of laser beam usually exceeds 200 nm and DSOM scanning step is usually 50 nm. Therefore, beam pointing to one pixel irradiates neighbouring pixels too and fluorophores from relatively large area are switched to dark state. It means that most of fluorophores would be already in the dark state before the centre of laser beam reaches their position unless their switching is reversible and activation is used. In case that photoswitching behaviour is irreversible, nearly no dynamic processes could be observed and the resolution would not be improvable by DSOM method.

5.1.2 Influence of laser power on switching rate

Influence of laser power on switching rate was tested to prove the theoretical prediction (Eqn. 5) that decrease of S_1 state population is excitation intensity dependent. Several experiments were done in which laser power of excitation was changed in range from 1 to 400 μW at sample. In Figure 5.3, there can be seen that the higher excitation intensity was used, the faster decay appeared. The intensity dependence was observed both for Dronpa and for rsFastLime.

To test, whether the switching rate is dependent on the integral excitation intensity (overall dose) another experiment was performed. The intensity of irradiation was kept the same, only pulses of different length were applied instead of continuous irradiation, thus changing the overall dose. The temporal resolution of our experiments is 200 μs. Within these 200 μs, the illumination can be arbitrarily switched on or off with down to tens of ns resolution using AOM device. In this experiment 2 μs long pulses were used with varying duty cycle from 100 ns to 1900 ns. This experiment showed that higher duty cycle (longer on time) of irradiation caused faster fluorescence decay (Figure 5.4). Switching kinetics is dependent on amount of absorbed photons.
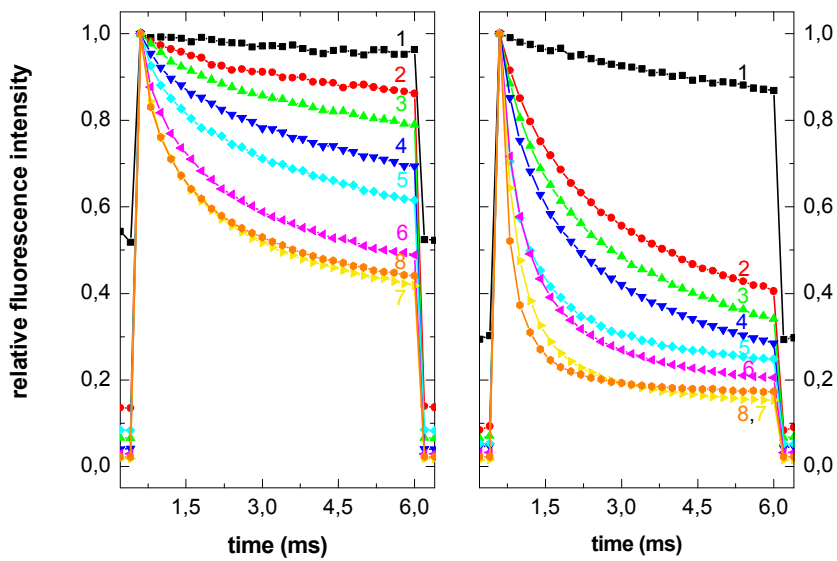
Figure 5.3 Influence of laser power on switching rate for Dronpa (left) and rsFastLime (right). Laser power (excitation): (1) 1 μW, (2) 5 μW, (3) 10 μW, (4) 20 μW, (5) 50 μW, (6) 100 μW, (7) 200 μW, (8) 400 μW. The higher excitation intensity the faster fluorescence decay.
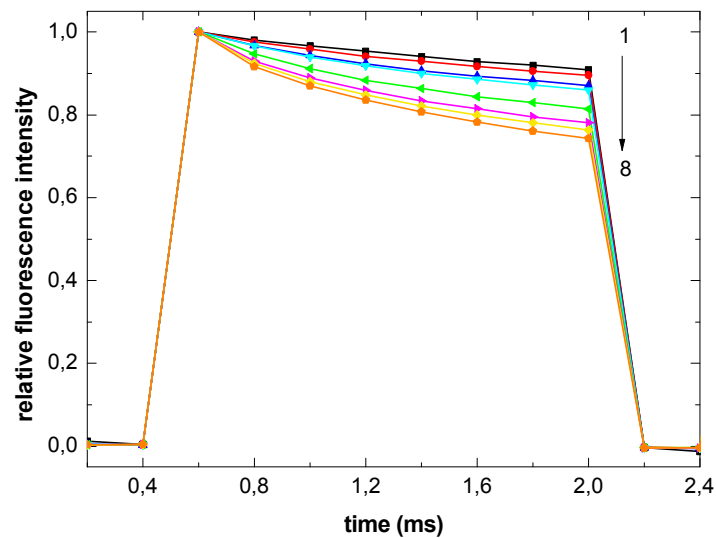

Figure 5.4. Influence of excitation light pulse duty cycle on decay kinetics of Dronpa. Pulse length is 2000 ns, on times are: (1) 100 ns, (2) 200 ns, (3) 300 ns, (4) 400 ns, (5) 600 ns, (6) 800 ns, (7) 1200 ns, (8) 1900 ns. Total number of pulses per read-out (200 μs) is 100. The longer on time the faster fluorescence decay.

DSOM requirement that irradiation with higher excitation intensities causes faster fluorescence decays is fulfilled for both Dronpa and rsFastLime switching. This means that in the centre of focused laser beam fluorescence decays will be faster than on its edges.

In our case, the choice of experimental excitation intensity depends mainly on time resolution of the microscope. It should be adjusted in such way that the fluorescence decay is properly sampled, but total measurement time kept as short as possible. In case, the time resolution of the microscope is freely adjustable, sample factors like photobleaching, triplet state formation and cell viability would come into play. If these processes were linearly dependent on irradiation, very high intensities and short measurement times could be applied. But as these processes are usually higher order in respect to photon flux, they would intensify significantly and hamper the measurement. Photodestruction of fluorophores is analysed in next chapter.

5.1.3 Determining of fluorophore photostability

The disadvantage of fluorescent proteins is that they easily undergo photodestruction (photobleaching). The stability of Dronpa proteins was tested so that the chosen area was consecutively scanned five times. The decrease of intensity at first point of fluorescence decay was monitored and plotted in Figure 5.5. The measurement was repeated for various excitation intensities. The higher intensity of excitation is the more proteins bleach. This dependence was observed for both Dronpa and rsFastLime. The measure of destruction is comparable for both proteins. As rsFastLime switching is more efficient than Dronpa switching (Figure 5.3) [29], rsFastLime undergoes more cycles between bright and dark states than Dronpa during the same illumination and scanning conditions. rsFastLime thus has lower photobleaching rate per cycle, although having similar overall photobleaching rate.
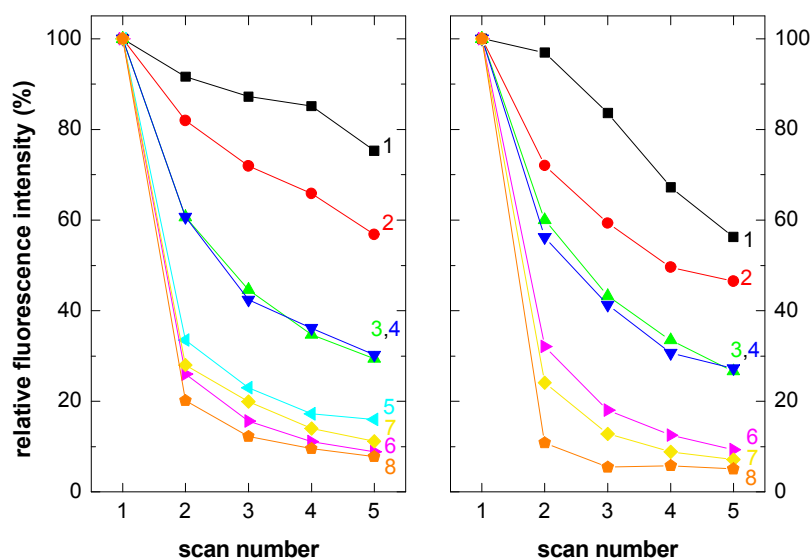
Figure 5.5. Influence of laser power on fluorophore stability. Decrease of fluorescence signal during repeated scanning for Dronpa (left) and rsFastLime (right). Laser power (excitation): (1) 1 µW, (2) 5 µW, (3) 10 µW, (4) 20 µW, (5) 50 µW, (6) 100 µW, (7) 200 µW, (8) 400 µW.

Photobleaching is a usual unpleasant effect in fluorescence microscopy. It is especially true for DSOM, because even moderate intensities (as 10 µW) cause serious photodestruction. The number of detectable photons per cycle and number of cycles per average lifetime of Dronpa molecule dictate the physical limits of DSOM method. Lowering of excitation intensity prevents from photobleaching but it does not help much in our case, because lower excitation intensity also decreases the number of detected photons, slows down the decay rates and thus overall DSOM performance remains the same.

5.1.4 Influence of activation intensity on fluorescence intensity

Activation light causes Dronpa return from the dark state to the ground state. Amount of absorbed light should influence the amount of molecules that come back to ground state and can be excited again. If more molecules return to ground state then the fluorescence signal should be higher. In following experiment, two activation periods with different powers of UV light and two excitation periods with the same intensities were applied. The experiment was repeated for different powers of UV light during first activation period. By evaluating maximum intensity of first fluorescence decay it was observed how the activation intensity changes the fluorescence intensity. This maximum value of

36

first decay was compared with maximum intensity of second fluorescence decay, which was activated and excited with the unvaried powers during all measurements. The ratio of maxima is plotted in Figure 5.6. At first, increasing of activation power causes the linear increase of fluorescence intensity. However, higher powers in range between 2 and 5 μW in the performed experiment do not increase fluorescence signal in a significant way anymore. Intensities from this "full activation" interval should be used in DSOM experiment because they maximise number of active molecules, which means more photons and better signal to noise. To avoid redundant irradiation, powers from the lower end of "full activation" interval should be used.
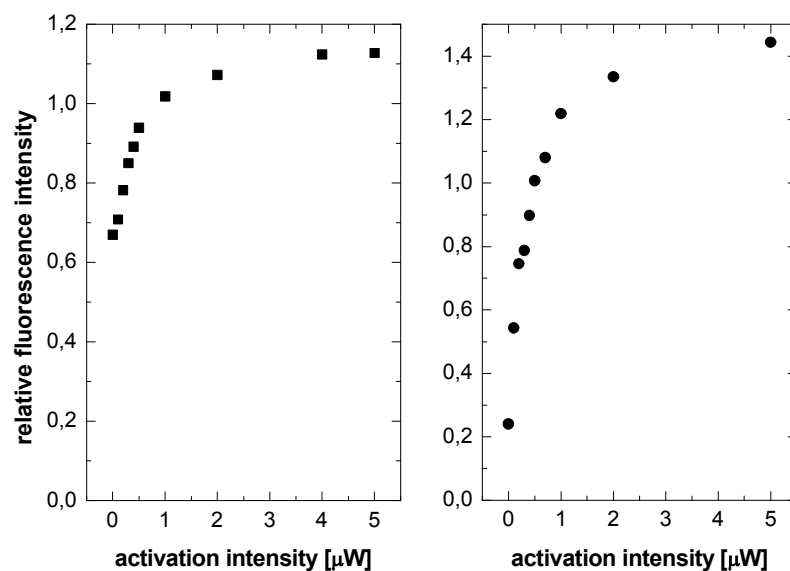

Figure 5.6. Influence of activation intensity on fluorescence intensity for Dronpa (left) and rsFastLime (right).

In another experiment, four excitation periods and four variously long activation periods were applied. The intensity of excitation and also of activation was unchanged during the whole experiment. Only the length of activation period was varied and lasted: 200 μs, 400 μs, 800 μs and 1,6 ms. Figure 5.7 shows that the longer period of activation was applied the higher fluorescence intensity was observed. In principle, this is the same result as in the first paragraph of this chapter. The graph stresses the importance of activation. Decays are short but it can be seen that they reach the same level of fluorescence intensity (all decays reach steady-state after some time. It means that rate of formation and rate of relaxation of dark state is equal and constant fluorescent signal can be observed), so they can be compared. The relative decay

amplitude corresponding to difference between first and last intensity point of fluorescence decay is higher for longer activation period. High relative amplitudes are favourable for DSOM because the decays can be better distinguished from constant offset, increasing signal to noise ratio. Therefore, the activation has to be sufficient for DSOM experiments.
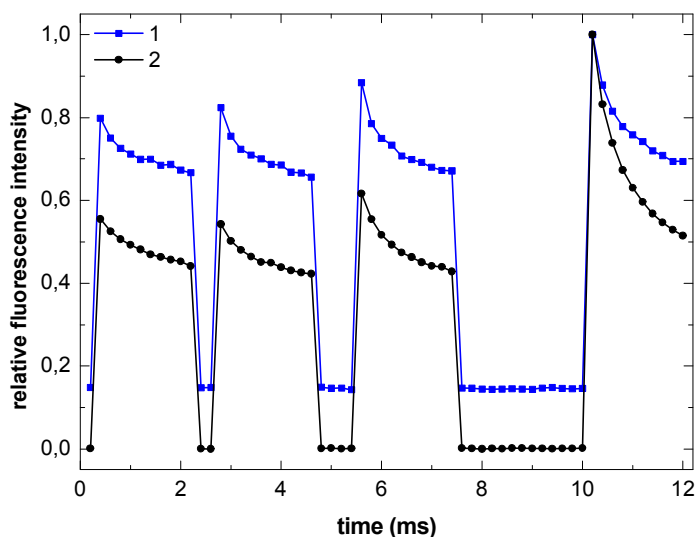

Figure 5.7. Various lengths of activation period. (1) Dronpa, (2) rsFastLime. The longer activation period, the higher fluorescence intensity. Activation power: 1 μW for Dronpa, 0,5 μW for rsFastLime.

One of the unanswered questions is what time the activation process needs to fully happen. The main concern is whether this time is longer than tens of microseconds or not. Unfortunately, we did not fully answer this question before finishing this work but we will continue in research on this topic. Activation process involves change of configuration and proton transfer. The process is efficient but it is not known how fast it can turn up. We only tried experiment in which we applied short activation period (lasting 200 or 400 μs) in different times before excitation period (800, 600, 400 or 200 μs before excitation), but high laser powers were used (7 μW activation, 56 μW excitation). The measure of activation was the same for all temporal positions of activation period. In future experiments, the time between activation and excitation period will be prolonged (up to 10 ms) and applied laser powers decreased to optimal levels. The case when activation process needs time to fully happen is unlucky for DSOM method because the measurements would have to be elongated, waiting for full

activation. Otherwise, the delayed activation would compete with deactivation and degrade the decay measurements.

5.1.5 Effect of excitation wavelength on switching rate

In this experiment excitation wavelength was changed. Used wavelengths were 458, 466, 473, 477, 488 a 497 nm. At first, just excitation wavelength was changed but irradiation intensity was kept equal for all measurements. It was observed that irradiation with longer wavelengths causes faster decays (Figure 5.8).
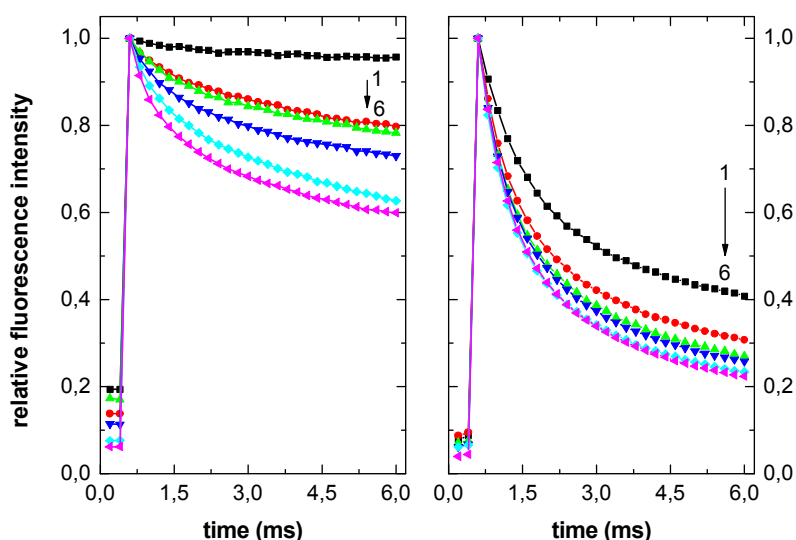

Figure 5.8. Influence of excitation wavelength on switching kinetics for Dronpa (left) and rsFastLime (right). Excitation wavelengths: (1) 458 nm, (2) 466 nm, (3) 473 nm, (4) 477 nm, (5) 488 nm, (6) 497 nm. The longer wavelength the faster fluorescence decay.

This result has two reasons. The first is that Dronpa has absorption maximum at 503 nm (rsFastLime at 496 nm). Longer wavelengths correspond to higher molar absorption coefficient so more photons are absorbed and switching to dark state is faster. The second reason is that shorter wavelengths are able to act also as activators. It means that they enable return from the dark state to the ground state similarly as ultraviolet light. Activation process goes against the switching process and the measured fluorescence decay is slowed down. Activation behaviour was observed in the experiment in which excitation period of shorter wavelength was alternated with excitation period of standard wavelength (488 nm). Irradiation intensities were chosen so that the sum of fluorescence signal recorded during excitation period with shorter wavelength and sum

of fluorescence signal recorded during excitation period with standard wavelength were nearly the same. Very weak activation periods were applied (< 60 nW). Figure 5.9 shows fluorescence decay after irradiation with standard wavelength and increase of fluorescence signal after irradiation with shorter wavelength (466 nm). The same behaviour was observed for other shorter wavelengths (Figure 5.9, right), the effect was not so pronounced for wavelength of 476 nm.
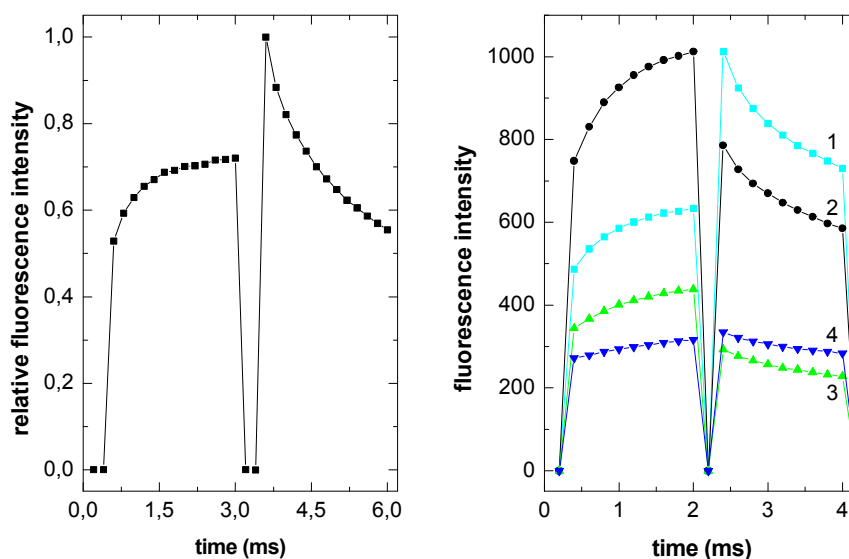

Figure 5.9. Influence of excitation wavelength on fluorescence signal of Dronpa. Both graphs show the same effect, on the left graph only one curve is shown for clearness. Left: Excitation wavelengths were 466 nm in first excitation period and 488 nm in second excitation period. Right: Excitation wavelengths were (1) 458 nm, (2) 466 nm, (3) 473 nm, (4) 477 nm in first excitation period and 488 nm in second excitation period. Absolute fluorescence signal is shown. Sum of fluorescence signal in first excitation period is higher or comparable with sum of signal in second excitation period (except 458 nm). No UV light was used in right graph, < 60 nW was used in left graph. More molecules are switched to dark state after irradiation with 488 nm. Higher fraction of molecules stays in bright state after irradiation with wavelengths shorter than 488 nm.

The increase of fluorescence intensity stops after some time and constant level of fluorescence signal is reached. It means that activation process competes with switching process and eventually rates of activation and switching processes equalize, reaching steady state. The probability of finding molecule in dark state D does not change anymore and this probability is different for different wavelengths. Higher probability can be found for longer wavelengths (488 and 497 nm) (Figure 5.10), lower probability for shorter wavelengths (< 488 nm). The reaching of steady state can be

accompanied by increase of fluorescence intensity ("activation process dominates"; as in this experiment) or by fluorescence decay ("switching process dominates"; other experiments with usage of UV light). This observation indicates that the absorption spectrum of dark state spans almost till the excitation maximum. The presented experiment may serve as an indirect method for measuring dark state absorption spectra.
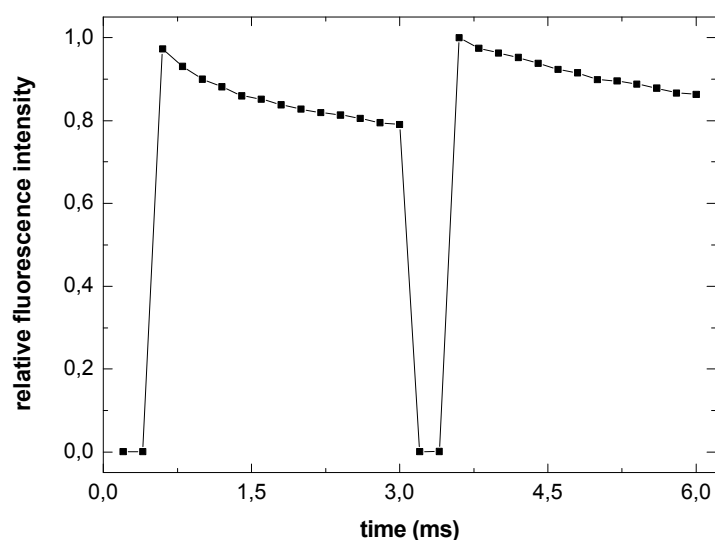

Figure 5.10. Influence of excitation wavelength on fluorescence signal of Dronpa. Excitation wavelengths were 497 nm in first excitation period and 488 nm in second excitation period. Very weak UV light was used (< 60 nW). More molecules are switched to dark state after irradiation with 497 nm than with 488 nm. Decays are not very rapid because low irradiation intensities were used.

The significant activation behaviour of shorter wavelengths slows down the fluorescence decay and is undesirable for DSOM experiments. Instead, longer wavelengths should be used preferentially to get the highest relative amplitude of fluorescence decay.

Choice of excitation wavelength is important not only for DSOM experiments but also for other super resolution methods as PALM or STED. These methods may also use photoswitching species for controllable turning on and off. Key point for obtaining high resolution with these techniques is to turn off the desired molecules completely. As was already written, the excitation wavelength determines the ratio of molecules in dark and bright states. If the ratio is not completely shifted in favour of the dark state, high background caused by bright molecules lowers achievable resolution. Irradiation with longer wavelengths causes that less molecules are in the bright state hence these wavelengths are more suitable for mentioned methods. The influence of

41

excitation wavelength on ratio of molecules in bright and dark state should also be considered when characterisation of Dronpa dark state is made, because probably no excitation wavelength is able to switch all molecules to the dark state (in bulk measurements). Even small amount of molecules remaining in the bright state can mystify the result.

5.1.6 Comparison of Dronpa's switching properties with other fluorescent proteins

Most of the above mentioned experiments were done for both rsFastLime and Dronpa. Previous chapters showed that fluorescence decays are faster for rsFastLime than for Dronpa under identical conditions, in agreement with theory [29]. These decays are compared with fluorescence decays of originally nonphotoswitchable green fluorescent protein (GFP) and with fluorescence signal from unlabelled yeast cells. The influence of irradiation intensity on switching rate is confronted. Fluorescence response of GFP in yeast cells and unlabelled cells to various excitation intensities are in Figure 5.11.
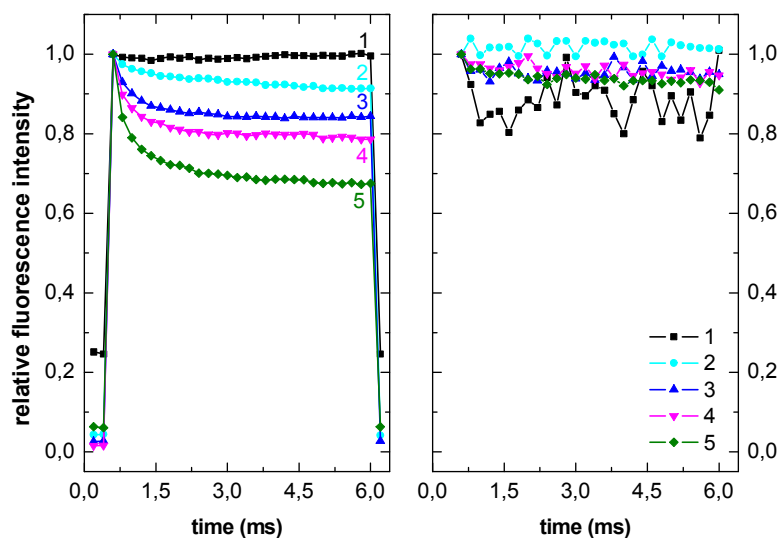

Figure 5.11. Influence of laser power on fluorescence decay of GFP (left) and unlabelled yeast cells (right). Laser powers: (1) 1 µW, (2) 5 µW, (3) 10 µW, (4) 20 µW, (5) 100 µW.

Unlabelled yeast cells do not manifest any fluorescence decay. In case of GFP, rapid but not strong fluorescence decay can be observed. The decay is also caused due to formation of some kind of dark state. FCS studies [36] showed that GFP undergoes photoinduced transitions between bright and dark states in the microsecond to

millisecond time-range. Our experiments probably detect this kind of transition. Comparison of Dronpa with GFP should show how other fluorescent protein reacts to applied laser sequence and also uniqueness of Dronpa. Observation of fluorescence decay due to formation of some kind of GFP dark state looks promising for DSOM usage but the problem is that the relative amplitude corresponding to GFP decay is small. Moreover, steady-state is reached very rapidly and the resulting decay is thus difficult to be properly sampled with current 200 μs time resolution. Dynamic transitions can not be observed after reaching of steady state, so photons, detected after reaching of steady state, can not improve the resolution of image. In the second section of Results and discussion part, the attempt for obtaining more resolved pictures using GFP is made.

Figure 5.12 shows fluorescence decays of various fluorescent proteins under identical conditions. The most rapid fluorescence decay is observed for rsFastLime, than for Dronpa and GFP, no decay is observed for unlabelled cells. Figure 5.12 (right) shows decays while experimental conditions for obtaining more resolved pictures were applied. GFP does not demonstrate any decay after irradiation with low powers. Acquiring of resolved images with GFP would demand higher excitation intensities. These experiments show that switching behaviour is not peculiar to unlabelled cells and can be ascribed to expressed fluorescent proteins.
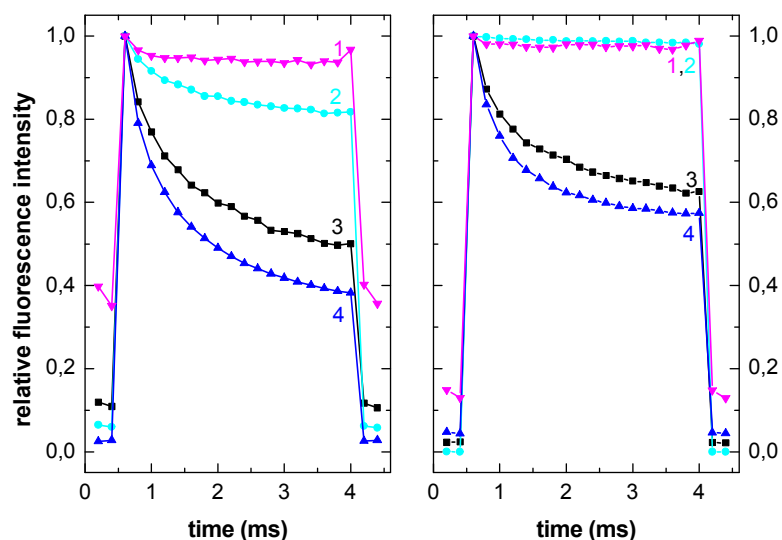
Figure 5.12 Comparison of decays of fluorescent proteins. (1) unlabelled yeast cells, (2) GFP, (3) Dronpa, (4) rsFastLime. Used laser powers were: 1 μW activation and 5 μW excitation for left graph, 0,15 μW activation and 2 μW excitation for right graph.

Note: Fluorescence decays are faster in comparison with Figure 5.3. This is because here the scanning step was 50 nm and 200 nm in Figure 5.3. The scanner is constantly moving during decay acquisitions. The bigger scanning step means that the scanner moves to area where more new unswitched molecules occur. These fresh molecules are initially in bright state so their appearance in confocal volume due to scanning slows down the apparent fluorescence decay.

5.1.7 Photoswitching on different time scales

Dronpa photoswitching is usually observed on millisecond to second time scale. However, the photoswitching mechanism probably involves more steps that occur on different time scales. Measurements done on faster times scale can contribute to the solution of switching mechanism. Moreover, knowing the fastest time scale on which suitable and well characterised photoswitching can happen may lead to faster DSOM image acquisition.

The change of experimental arrangement enables us to detect fluorescence signal with temporal resolution between 88 to 450 ns. This makes possible to study kinetics of photoswitching and to acquire images with decays on microsecond timescale. The main limitation of the "microsecond" experimental setup is that it allows only getting maximum 128 points per decay measurement with a dead time of 3 ms between consecutive readouts.

Experiments testing basic photoswitching behaviour on microsecond timescale were done. 50 μs decay was recorded every 3 ms with 450 ns time resolution, both activation and excitation periods were applied. Fluorescence decays demonstrated that they are intensity dependent but relatively high excitation intensities (13 μW and more) have to be used for manifesting of decay behaviour (Figure 5.13). The fluorescence decays are noisier due to lower amount of emitted and detected photons per time step.
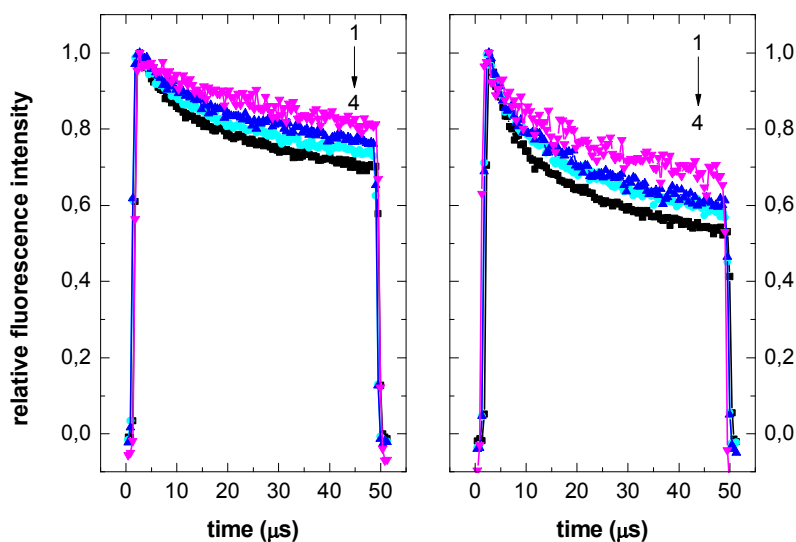

Figure 5.13. Fluorescence decays of Dronpa (left) and rsFastLime (right) on microsecond time scale. Excitation intensities: (1) 13 μW, (2) 33 μW, (3) 46 μW, (4) 66 μW.

In another experiment, influence of activation was tested. Activation period was applied before first, second and fourth fluorescence decays, but was missing before third fluorescence decay. Figure 5.14 shows that fluorescence signal of third decay is not as strong as in other decays, only partial recovery of fluorescence occurred. It means that activation by UV light influences switching behaviour on this timescale, activation helps to recover fluorescence signal. Partial recovery of fluorescence signal of the third decay can be explained by spontaneous return from dark states or by diffusion of new Dronpa molecules to the detection volume. In this experiment, the Dronpa molecules are attached to cytoplasmic protein and they are freely moving inside the cell. Time between measuring two decays (3 ms) is long enough for partial molecule exchange in the detection volume (molecules in bright state in place of molecules in dark state). These measurements do not provide any clear conclusion about the switching mechanism due to contribution of the diffusion. On the other hand, the measurements do not exclude the existence of spontaneous recovery from some kind of dark state to

45

the bright state. Dronpa's dark state is usually described as stable (relaxation half-time is 840 min (Table 3.1), it means that half of the molecules in dark state spontaneously switch to bright state in 840 min). Therefore spontaneous transition may occur from different kind of dark state, possibly from triplet state because of time scale and usage of higher irradiation powers. But this is only a speculation. More measurements have to be done on the sample with restricted Dronpa movement to confirm the observation of the triplet state.
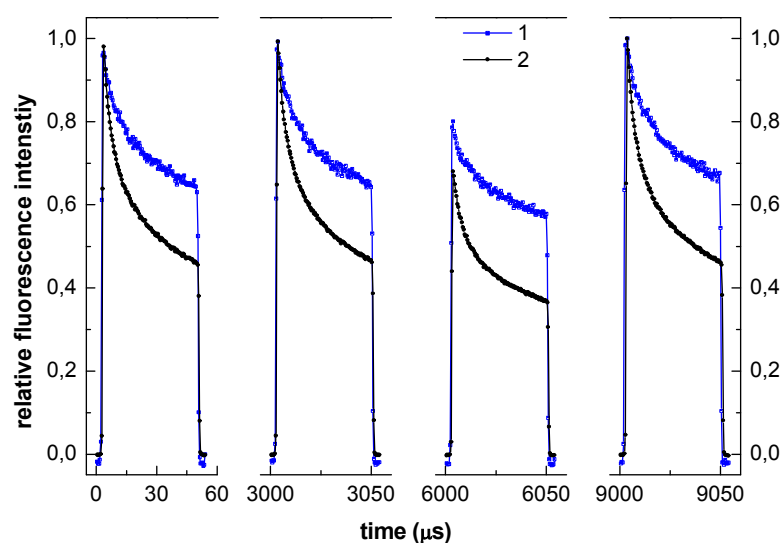

Figure 5.14. Fluorescence decays of (1) Dronpa and (2) rsFastLime on microsecond timescale. Decays were recorded every 3 ms. Except third decay, activation period was applied before excitation period.

Photoswitching behaviour on the microsecond time scale may be used for acceleration of measurement. At this time, our "microsecond" measurement setup is limited by camera dead time (3 ms) when the signal is read out and camera cannot collect any new photons. Measurements done on microsecond time scale presently cannot shorten overall acquisition time (for our setup). Nevertheless future implementation of so-called "crop" continuous data read out mode with 16 μs time resolution can potentially speed up image acquisition 10x compared to standard approach.

5.2 Acquiring of high resolution images

Results from the first part helped us to optimize experimental conditions for obtaining high resolution images. Dronpa attached to membrane protein of yeast cells was chosen

for imaging. Results from performed tests suggest that rsFastLime may be a better candidate due to comparable photostability and faster switching to dark state. Unfortunately, we had only cells with rsFastLime freely moving in mitochondria which size is typically about 1 μm. This size is larger than resolution limit, so this structure is inappropriate for showing of resolution improvement. Demonstration of resolution improvement is done on tiny structures, e.g. cell membrane with thickness of few nanometres. Based on previous experiments, experimental conditions were: low excitation intensities, activation intensities preferably from "full activation" interval, excitation wavelength 488 nm, millisecond timescale. Activation period lasted 400 μs, excitation period lasted 7,6 or 5,6 ms. Scanning step size was set to 50 nm. Acquiring of 100x100 pixels image lasted about two minutes.

5.2.1 Image creation

As soon as optimal experimental parameters were chosen DSOM images could be directly acquired. The obtained data represent 3D matrix with the fluorescence decay creating the third dimension. It can be treated in several ways. The total fluorescence signal for each pixel (decay in third dimension) can be summed up, giving confocal image with saturation effect. In further text let us call this image simply as a confocal image. The saturation effect caused by photoswitching generally lowers resolution. To get true confocal image without pronounced saturation effect, intensities at first point of fluorescence decays must be taken. Let us call this true confocal image. The true confocal image is the reference with which the resolution improvement must be compared with.

The obtained scanned image can be decomposed into three images (Figure 5.15, B-D) as was already described in the theoretical part. Amplitudes corresponding to fast decays form a high resolution image, amplitudes corresponding to slow decays and amplitudes corresponding to temporally non-resolved offset form additional low resolution images. Temporally constant offset comes from areas with constant intensity signal as autofluorescence from inner organelles, signal out of focal plane or noise. Slow transition kinetics is usually detected "on the border" of structures labelled with photoswitchable proteins. The separation of this signal (and also of constant offset) leads to sharper images.
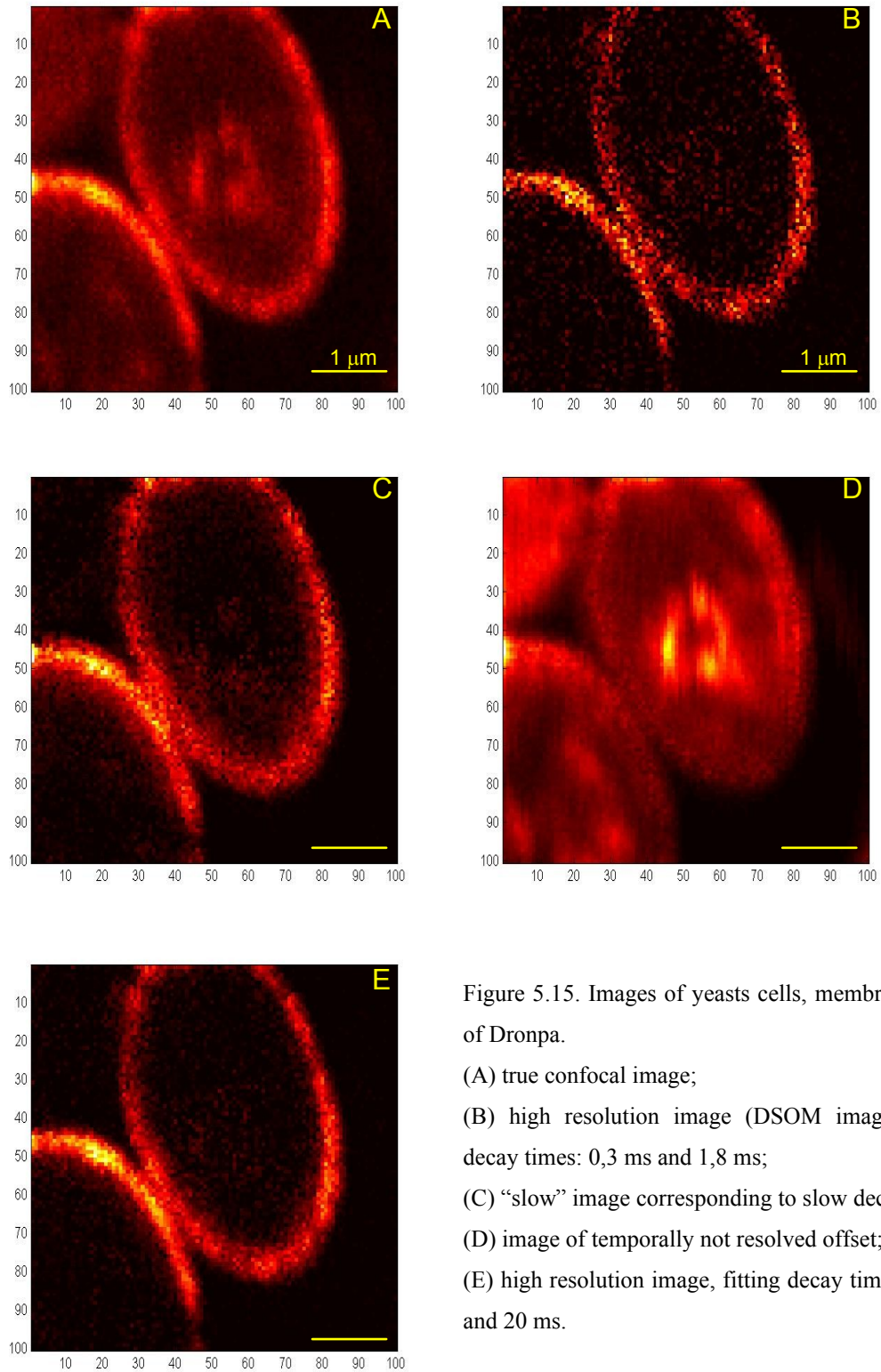
Figure 5.15. Images of yeasts cells, membrane signal of Dronpa.

(A) true confocal image;

(B) high resolution image (DSOM image), fitting decay times: 0,3 ms and 1,8 ms;

(C) "slow" image corresponding to slow decay time;

(D) image of temporally not resolved offset;

(E) high resolution image, fitting decay times: 0,3 ms and 20 ms.

5.2.2 Choice of fitting parameters

The data analysis requires the choice of fitting parameters, namely fast and slow decay time. First estimation of parameters was obtained by fitting averaged decay. This decay is an average of all decays from all pixels. Average decay is fitted to two-exponential model with offset and obtained decay times τ_{fast} and τ_{slow} are used for further analysis. Data (all decays from all pixels) are then fitted to two-exponential model (Eqn. 11) with given decay times. Amplitudes corresponding to fast transition kinetics creates the more resolved image. The cross-section was made in the resolved image and the intensity profile along this cross-section was monitored. Full width at half maximum was considered as obtainable resolution. The resolution was affected by choice of decay times. Therefore, decay times were varied and their influence on obtainable resolution was examined (Figure 5.16). Observed changes were of the same kind as in article of Jana Humpolíčková [8]. τ_{fast} determines the fastest decay time which can be distinguished. The change of this parameter does usually not influence the resolution significantly, only longer times cause worsening of resolution probably because of slow-decaying contributions. The parameter τ_{fast} can be used directly from the fit of average decay. However, τ_{slow} does influence the resolution. The larger the difference between τ_{fast} and τ_{slow} is the more photons (and so more variously fast contributions) form high resolution images. Images are then smoother but the resolution is worse. The smaller the difference between τ_{fast} and τ_{slow} is the better resolution is but the noisier the image becomes. The trade-off between resolution and image quality has to be made. τ_{slow} obtained directly from fit usually demonstrates nice improvement of resolution but it is desired to check whether usage of shorter time is able to improve the resolution even more. Prolongation of τ_{slow} to really long times (20 ms) does not demonstrate resolution enhancement but it makes images smoother and brighter (Figure 5.15, E). Important effect can be seen that structures labelled with photoswitchable proteins are highlighted and autofluorescence with noise is suppressed for any selection of decay times.
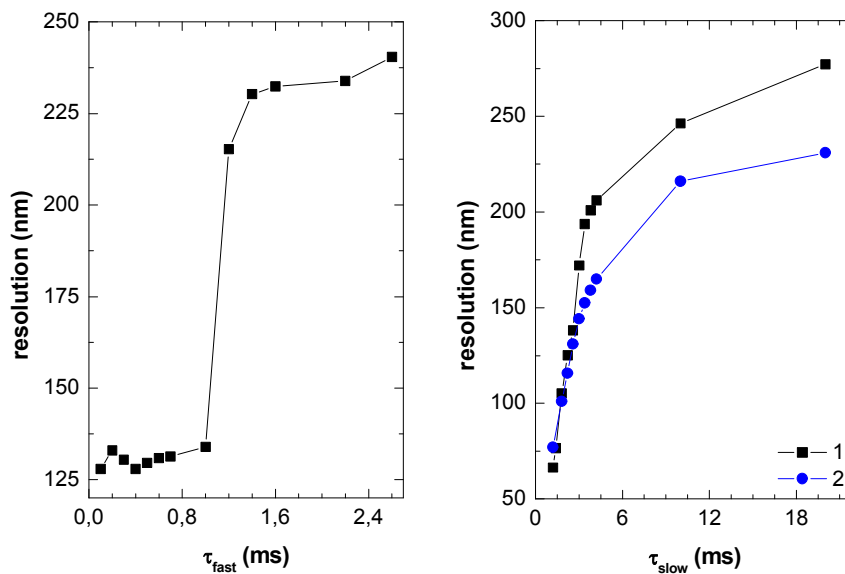
Figure 5.16. Variation of fitting parameters. Left graph shows the change of resolution due to variation of fast decay time (slow decay time was used from fit: 2,58 ms). Right graph shows dependence of obtainable resolution on slow decay time. Fast decays were (1) 1 ms and (2) 0,3 ms.

Figure 5.16 shows that resolution under 100 nm could be reached. It means that fitting procedure found relatively high "fast" amplitude in one scanned pixel, but there is no other like that in neighbourhood. Unfortunately, this does not fulfil Nyquist criterion (mentioned earlier) which says that every sample's feature should be collected by two pixels. Intensity profiles with such resolution were excluded from determining the best obtainable resolution.

It may seem that chosen scanning step (50 nm) is too large and that better resolution would be obtained by shortening of the step. But the shortening has its limitations. For example: 2x denser sampling (step size 25 nm), provided that the scanned area and the length (and power) of laser sequence were the same, means 4x longer measurement time resulting in about 4x more pronounced photobleaching. Moreover achieving two-times better resolution (50 nm) also means 8-times less photons contributing to the fast decay, increasing signal to noise ratio significantly and leading to very noisy pictures. The trade-off between obtainable resolution and measurement length or image quality has to be done. Absolute limits are set by sample photobleaching.

5.2.3 High resolution image

In this paragraph, true confocal and high resolution images are compared (Figure 5.15, Figure 5.17, A and B). At first glance, the fluorescence signal comes only from membrane where Dronpa was placed at DSOM image. It means that the autofluorescence signal from inner organelles is suppressed. Further, blurring inside the cells caused by signal out of focal plane is suppressed at DSOM image. This filtering can also be seen on cell in left corner of true confocal picture. The cell is partly visible in true confocal image and probably is out of focal plane. The cell disappeared in DSOM picture.

For comparison of resolution in true confocal and DSOM image, a cross-section was done in membrane area. An intensity profile along the cross-section was obtained and a full width at half maximum was measured. The DSOM profile (Figure 5.17, C) demonstrates that membranes are better separated. Especially, the membrane is distinguished better from signal coming from inside of the cell. DSOM profiles were usually up to two times narrower than true confocal profiles. The best resolution which was obtained was 100 nm.
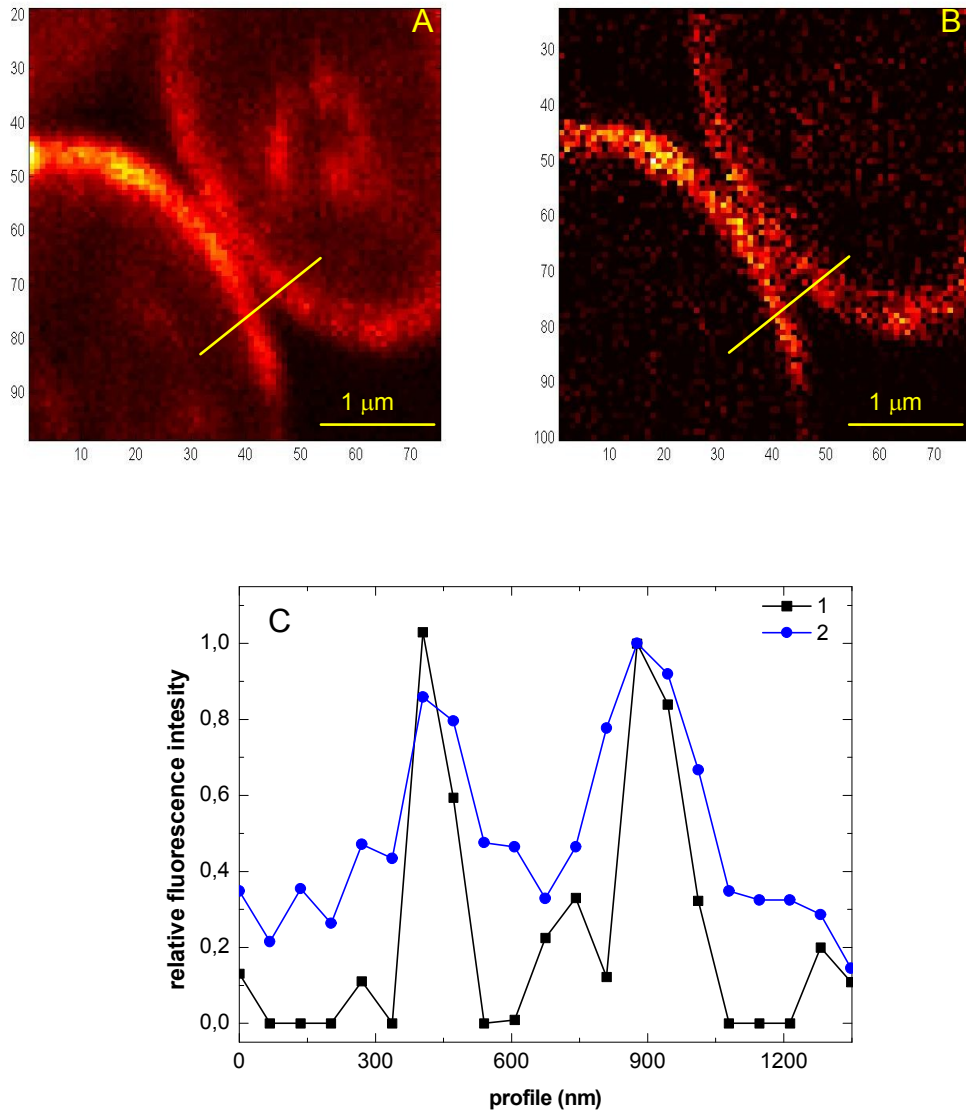
Figure 5.17. Detailed view of (A) true confocal image and (B) high resolution image,
(C) intensity profile for (1) high resolution and (2) true confocal image along cross-sections denoted in A
and B pictures. Full widths of half maximum for depicted two peaks:

Table 5.1

	Resolved profile (nm)	True confocal profile (nm)	Ratio
Left peak	108	368	3,41
Right peak	150	298	1,99

5.2.4 The testing of cells labelled with originally non-photoswitchable fluorescent protein for obtaining more resolved pictures

Fluorescence decay due to formation of dark state was also observed for GFP. Therefore, more resolved pictures were attempted to obtain (Figure 5.18). The attempt was not successful. Fitting procedure could distinguish cells but it did not separate GFP fluorescence signal from autofluorescence signal very well. Part of dead cell on the bottom of true confocal image was filtered out but the cell on right side remained. Even prolongation of slow decay time did not suppress autofluorescence. The improvement of resolution could be observed in only restricted areas. Intensity profiles were often noisy. The reason why GFP switching is not usable for DSOM probably is that the decays reach steady state very rapidly. This may indicate a fast autorecovery which lessens the dependence of decay rate on excitation intensity and by this disables obtaining high resolution images. The low decay amplitude also causes that the pictures are noisier.

The reversible and controllable photoswitching of Dronpa with low spontaneous recovery is essential for DSOM method.
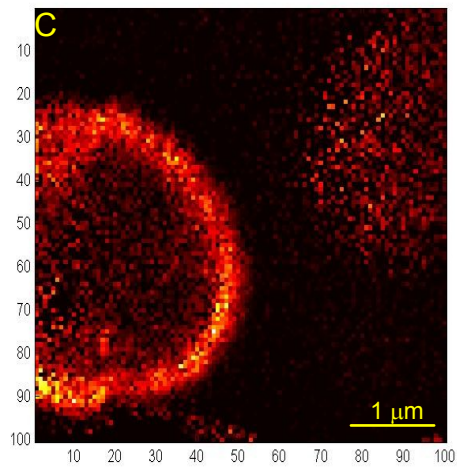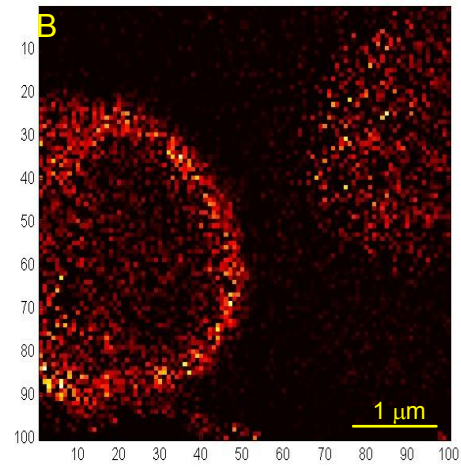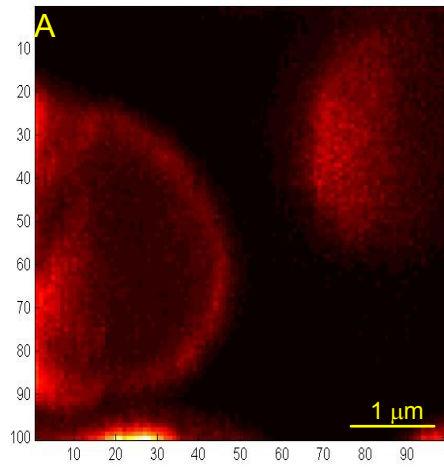
Figure 5.18. Images of yeasts cells, membrane signal of GFP.

(A) true confocal image;

(B) resolved image, fitting decay times: 0,18 ms and 0,96 ms;

(C) resolved image, fitting decay times: 0,18 ms and 20 ms.

6 Conclusions

In this work, high resolution images of biological samples were obtained by DSOM method. This goal was accomplished thanks to characterisation of Dronpa properties:

- The photoswitching behaviour of Dronpa was confirmed.

- The dependence of switching kinetics on intensity of excitation light was observed. The higher excitation intensity the faster fluorescence decay. This conclusion is in agreement with theory.

- Photostability of fluorophore was tested, medium to lower irradiation powers were recommended.

- The transition kinetics was also influenced by excitation wavelength. Irradiation with longer wavelengths caused faster fluorescence decays. Shorter wavelengths act also as activators screening out the fluorescence decay. The steady-state ratio of molecules in dark and bright state depends on irradiation wavelength. DSOM prefers longer wavelengths.

- Obtainable fluorescence signal is influenced by activation process. Sufficient intensity of activation should be used for effective return of Dronpa molecules to bright state. The more molecules are in bright state the higher relative amplitude is observed in decay and this decay is better distinguished from noise in DSOM fitting procedure.

- The switching between fluorescent and non-fluorescent states was observed both on millisecond and on microsecond time scales.

- Dronpa decays were compared with decays of Dronpa mutant rsFastLime, green fluorescent protein and with fluorescent signal of unlabelled cells. rsFastLime manifested faster switching and comparable photostability than Dronpa. GFP also showed fluorescence decay which reached its steady state very rapidly. Unlabelled cells did not show any switching behaviour.

Characterisation experiments demonstrated that Dronpa and rsFastLime are suitable fluorophors for DSOM experiments. Moreover, they enabled optimization of experimental conditions for acquiring high resolution images. The high resolution DSOM images were acquired with following results:

- Two times better resolved images of yeast cell membrane were obtained. Choice of fitting parameters influenced obtainable resolution. The best resolution achieved was 100 nm in focal plane.
- Autofluorescence was suppressed. Smooth images of membrane were obtained after prolongation of slow decay time during fitting procedure.
- Signal out of focal plane was filtered out.
- The GFP switching was not usable for obtaining high resolution images.

7 Bibliography

[1]   Abbe E. Beiträge zur Theorie des Mikroskops und der mikroskopischen Wahrnehmung. *Archiv für mikroskopische Anatomie* (1873) **9**: pp. 413-418.

[2]   Rittweger E, Han KY, Irvine SE, Eggeling C & Hell SW. STED microscopy reveals crystal colour centres with nanometric resolution. *Nat Photonics* (2009) **3**: pp. 144-147.

[3]   Betzig E, Patterson GH, Sougrat R, Lindwasser OW, Olenych S, Bonifacino JS, Davidson MW, Lippincott-Schwartz J & Hess HF. Imaging intracellular fluorescent proteins at nanometer resolution. *Science* (2006) **313**: pp. 1642-1645.

[4]   Hein B, Willig KI & Hell SW. Stimulated emission depletion (STED) nanoscopy of a fluorescent protein-labeled organelle inside a living cell. *Proc Nat Acad Sci Usa* (2008) **105**: pp. 14271-14276.

[5]   Gustafsson MGL. Surpassing the lateral resolution limit by a factor of two using structured illumination microscopy. *J Microsc-Oxford* (2000) **198**: pp. 82-87.

[6]   Yamanaka M, Kawano S, Fujita K, Smith NI & Kawata S. Beyond the diffraction-limit biological imaging by saturated excitation microscopy. *J Biomed Opt* (2008) **13**: .

[7]   Dertinger T, Colyer R, Iyer G, Weiss S & Enderlein J. Fast, background-free, 3D super-resolution optical fluctuation imaging (SOFI). *Proc Nat Acad Sci Usa* (2009) **106**: pp. 22287-22292.

[8]   Humpolickova J, Benda A, Machan R, Enderlein J & Hof M. Dynamic saturation optical microscopy: employing dark-state formation kinetics for resolution enhancement. *Phys Chem Chem Phys* (2010) **12**: pp. 12457-12465.

[9]   Enderlein J. Breaking the diffraction limit with dynamic saturation optical microscopy. *Appl Phys Lett* (2005) **87**: .

[10]   Ando R, Mizuno H & Miyawaki A. Regulated fast nucleocytoplasmic shuttling observed by reversible protein highlighting. *Science* (2004) **306**: pp. 1370-1373.

[11]   Schermelleh L, Heintzmann R & Leonhardt H. A guide to super-resolution fluorescence microscopy. *J Cell Biol* (2010) **190**: pp. 165-175.

[12]   Heintzmann R & Ficz G. Breaking the resolution limit in light microscopy. *Briefings in Functional Genomics and Proteomics* (2006) **5**: pp. 289-301.

[13]   Hell SW & Wichmann J. Breaking the diffraction resolution limit by stimulated-emission-depletion fluorescence microscopy. *Optics Letters* (1994) **19**: pp. 780-782.

[14]   Humpolickova J, Benda A & Enderlein J. Optical Saturation as a Versatile Tool to Enhance Resolution in Confocal Microscopy. *Biophys J* (2009) **97**: pp. 2623-2629.

[15]   Fujita K, Kobayashi M, Kawano S, Yamanaka M & Kawata S. High-resolution confocal microscopy by saturated excitation of fluorescence. *Phys Rev Lett* (2007) **99**: .

[16]   Hess ST, Girirajan TPK & Mason MD. Ultra-high resolution imaging by fluorescence photoactivation localization microscopy. *Biophys J* (2006) **91**: pp. 4258-4272.

[17]   Rust MJ, Bates M & Zhuang XW. Sub-diffraction-limit imaging by stochastic optical reconstruction microscopy (STORM). *Nat Methods* (2006) **3**: pp. 793-795.

[18]   Pawley JB. HANDBOOK OF BIOLOGICAL CONFOCAL MICROSCOPY, Third edition. Springer Science+Business Media, LLC, 2006.

[19]   Heilemann M, Dedecker P, Hofkens J & Sauer M. Photoswitches: Key molecules for subdiffraction-resolution fluorescence imaging and molecular quantification. *Laser Photonics Rev* (2009) **3**: pp. 180-202.

[20]   Patterson GH & Lippincott-Schwartz J. A photoactivatable GFP for selective photolabeling of proteins and cells. *Science* (2002) **297**: pp. 1873-1877.

[21]   Wiedenmann J, Ivanchenko S, Oswald F, Schmitt F, Rocker C, Salih A, Spindler KD & Nienhaus GU. EosFP, a fluorescent marker protein with UV-inducible green-to-red fluorescence conversion. *Proc Nat Acad Sci Usa* (2004) **101**: pp. 15905-15910.

[22]   Heilemann M, Margeat E, Kasper R, Sauer M & Tinnefeld P. Carbocyanine dyes as efficient reversible single-molecule optical switch. *J Am Chem Soc* (2005) **127**: pp. 3801-3806.

[23]   Bates M, Huang B, Dempsey GT & Zhuang XW. Multicolor super-resolution imaging with photo-switchable fluorescent probes. *Science* (2007) **317**: pp. 1749-1753.

[24]   Irie M, Fukaminato T, Sasaki T, Tamai N & Kawai T. Organic chemistry: A digital fluorescent molecular photoswitch. *Nature* (2002) **420**: pp. 759-760.

[25]   Minkin VI. Photo-, thermo-, solvato-, and electrochromic spiroheterocyclic compounds. *Chem Rev* (2004) **104**: pp. 2751-2776.

[26]   . Amalgaam Co., Ltd.:
"http://www.amalgaam.co.jp/products/coral_hue/Photoconvertible/dronpa_green .html", cited 1.5.2011.

[27]   Andresen M, Stiel AC, Folling J, Wenzel D, Schonle A, Egner A, Eggeling C, Hell SW & Jakobs S. Photoswitchable fluorescent proteins enable monochromatic multilabel imaging and dual color fluorescence nanoscopy. *Nat Biotechnol* (2008) **26**: pp. 1035-1040.

[28]   Hofmann M. RESOLFT-Mikroskopie mit photoschaltbaren Proteinen (PhD thesis) . Doctoral dissertation, Ruprecht - Karls - Universität Heidelberg.2007.

[29]   Stiel AC, Trowitzsch S, Weber G, Andresen M, Eggeling C, Hell SW, Jakobs S & Wahl MC. 1.8 angstrom bright-state structure of the reversibly switchable fluorescent protein Dronpa guides the generation of fast switching variants. *Biochem J* (2007) **402**: pp. 35-42.

[30]   . RCSB Protein Data Bank:
"http://www.rcsb.org/pdb/explore/explore.do?structureId=2Z1O", cited 1.5.2011.

[31]   Andresen M, Stiel AC, Trowitzsch S, Weber G, Eggeling C, Wahl MC, Hell SW & Jakobs S. Structural basis for reversible photoswitching in Dronpa. *Proc Nat Acad Sci Usa* (2007) **104**: pp. 13005-13009.

[32]   Mizuno H, Mal TK, Walchli M, Kikuchi A, Fukano T, Ando R, Jeyakanthan J, Taka J, Shiro Y, Ikura M & Miyawaki A. Light-dependent regulation of structural flexibility in a photochromic fluorescent protein. *Proc Nat Acad Sci Usa* (2008) **105**: pp. 9227-9232.

[33]   Ebisawa T, Yamamura A, Kameda Y, Hayakawa K, Nagata K & Tanokura M. The structure of mAG, a monomeric mutant of the green fluorescent protein Azami-Green, reveals the structural basis of its stable green emission. *Acta Crystallogr F-Struct Bio* (2010) **66**: pp. 485-489.

[34]   Dedecker P, Hotta J, Ando R, Miyawaki A, Engelborghs Y & Hofkens J. Fast and reversible photoswitching of the fluorescent protein Dronpa as evidenced by fluorescence correlation spectroscopy. *Biophys J* (2006) **91**: pp. L45-L47.

[35]   Habuchi S, Dedecker P, Hotta JI, Flors C, Ando R, Mizuno H, Miyawaki A & Hofkens J. Photo-induced protonation/deprotonation in the GFP-like fluorescent protein Dronpa: mechanism responsible for the reversible photoswitching. *Photochem Photobiol Sci* (2006) **5**: pp. 567-576.

[36]   Widengren J, Mets U & Rigler R. Photodynamic properties of green fluorescent proteins investigated by fluorescence correlation spectroscopy. *Chem Phys* (1999) **250**: pp. 171-186.